Intersectin goes nuclear: secret life of an endocytic protein

Gualtiero Alvisi‡*, Lucia Paolini†, Andrea Contarini‡, Chiara Zambarda†, Veronica Di Antonio‡, Antonella Colosini†, Nicole Mercandelli†, Martina Timmoneri‡, Giorgio Palù‡, Luigi Caimi†, Doris Ricotta† and Annalisa Radeghieri†*

‡Department of Molecular Medicine, University of Padua, Padua, Italy

†Department of Molecular and Translational Medicine, University of Brescia, Brescia, Italy

*Corresponding authors:

Annalisa Radeghieri, Department of Molecular and Translational Medicine, University of Brescia, Viale Europa 11, 25123 Brescia, Italy. Phone number: 0039-030-3717543, Fax number: 0039-030-3717531 E-mail: annalisa.radeghieri@unibs.it

Gualtiero Alvisi, Department of Molecular Medicine, University of Padua, Padua, Italy, Via Gabelli 63, 35121 Padova, Italy. Phone number: 0039-049-8272353, Fax number: 0039-049-8272355 E-mail: gualtiero.alvisi@unipd.it

ORCID

GA orcid.org/0000-0002-8177-3616

LP orcid.org/0000-0002-4410-5272

CZ orcid.org/0000-0003-3730-8896

GP orcid.org/0000-0002-6310-5147

LC orcid.org/0000-0002-7163-9405

DR orcid.org/0000-0002-2217-3012

AR orcid.org/0000-0003- 2737-1090

Abstract

Intersectin 1-short (ITSN1-s) is a 1220 amino acids ubiquitously-expressed scaffold protein presenting a multi-domain structure that allows to spatiotemporally regulate the functional interaction of a plethora of proteins. Beside its well-established role in endocytosis, ITSN1-s is involved in regulation of cell signaling and is implicated in tumorigenesis processes, although the signaling pathways involved are still poorly understood. Here we identify ITSN1-s as a nucleocytoplasmic trafficking protein. We show that, by binding to importin (IMP)α, a small fraction of ITSN1-s localizes in the cell nucleus at the steady state, where it preferentially associates with the nuclear envelope (NE) and interacts with lamin A/C. However, upon pharmacological ablation of Chromosome region maintenance 1 (CRM-1) dependent nuclear export pathway, the protein accumulates into the nucleus, thus revealing its moonlighting nature. Analysis of deletion mutants revealed that the coiled coil (CC) and Src homology (SH3) regions play the major role in its nucleocytoplasmic shuttling. While no evident nuclear localization signal (NLS) was detected in the CC region, a functional bipartite NLS was identified within the SH3D region of ITSN1-s (**RKK**NPGGWWEGELQA**R**G**KKR**QIGW-1127), capable of conferring energy-dependent nuclear accumulation to reporter proteins and whose mutational ablation affects nuclear import of the whole SH3 region. Thus, ITSN1-s is an endocytic protein, which shuttles between the nucleus and the cytoplasm in a CRM-1 and IMPα dependent fashion.

Introduction

Scaffold proteins **(**scaffolds), are important components of several cellular processes and signaling systems. Usually, scaffolds are soluble proteins devoid of enzymatic activity, containing several modular protein-interaction domains within their structure, together with sites for inducible posttranslational modifications [1]. Scaffolds control the assembly of multiprotein complexes, thus contributing to localize signaling molecules to specific cell compartments or/and to regulate the efficiency of signaling pathways [2]. For example, Grb2-Associated Binding Protein 2 (GAB2) is involved in the assembly of signaling systems downstream of receptor tyrosine kinases and non-receptor tyrosine kinases [3], while Shc proteins have roles in signaling via many different types of receptors, such as growth factor receptors, antigen receptors, cytokine receptors, G-protein coupled receptors, hormone receptors and integrins [4].

Accumulating evidence suggests that several cytoplasmic adaptor proteins involved in endocytosis, such as clathrin, adaptor protein containing a pleckstrin homology domain, phosphotyrosine-binding domain, and leucine zipper motif 1 (APPL1) and Beta arrestin1, are capable of shuttling between the nucleus and the cytoplasm, being involved in nuclear signaling and transcriptional events in response to extracellular signals [5-7]. Therefore, a detailed understanding of the cellular compartmentalization dynamics of adaptor proteins is crucial to gain insights regarding their function.

In eukaryotes, nucleocytoplasmic transport of cargoes larger than 50-60 kDa is a signal- and energy-dependent process, which takes place across aqueous channels, delimited by nuclear envelope (NE)-embedded nuclear pore complexes (NPCs). Members of the kariopherin superfamily, recognize specific nuclear targeting signals (NTSs) responsible for targeting cargoes either into or out of the nucleus, nuclear localization or nuclear export signals - NLSs and NESs - respectively [8]. Usually nuclear import is mediated by importins (IMPs), such as IMPβ1 or one of its homologues, after recognition of cargo bearing NLSs, either directly or through the adaptor molecule IMPα. IMPα recognizes short basic NLSs - also named "classical" NLS (cNLS). cNLSs can be classified as monopartite - matching the consensus K-(K/R)-X-(K/R), or bipartite - matching the consensus: [(K/R)(K/R)–$X_{10–12}$–$(K/R)_{3/5}$], where X is any amino acid, and $(K/R)_{3/5}$ represents 3 lysine or arginine residues out of 5 consecutive amino acids. Subsequently, complexes are translocated through the NPCs into the nucleus, whereby binding of RanGTP to IMPβ promotes their dissociation and cargo release [9].

On the other hand, proteins are exported from the nucleus by exportins such as Chromosome region maintenance 1 (CRM-1), the so far best characterized exportin. In the nucleus, RanGTP-complexed CRM-1 recognizes cargoes bearing short NESs containing four non-consecutive

hydrophobic residues [10] and it translocates them to the cytoplasm, where RanGTP-CRM1-cargo complexes are dissociated and RanGTP is hydrolyzed to RanGDP and this allows CRM1 to be recycled back to the nucleus [11].

Intersectin 1 (ITSN1) is a ubiquitously expressed scaffold protein present in a long and short isoform of 190 and 145 kDa respectively. ITSN1-s contains two N-terminal Eps15 homology (EH) domains, a coiled coil (CC) region, and five SRC homology 3 (SH3A-E) domains. Due to its multimodular architecture, it interacts with several proteins involved in clathrin- and caveolin-mediated endocytosis, rearrangements of the actin cytoskeleton, cell signaling and survival [12, 13]. Indeed EH domains recognize the Asn-Pro-Phe (NPF) motif of many endocytic machinery proteins, including Epsin [14, 15] while the coiled coil (CC) region mediates protein dimerization and interacts with Eps15 and Eps15R [16], as well as with SNAP23, SNAP25 and HIP [17]. The SH3 domains, typical of cytoskeleton proteins and proteins involved in signal transduction, recognize proline rich motifs of endocytic proteins such as Dynamin, Synapsin and Synaptojanin [18], as well as the SH3 domain of Endophilin [19].

Analysis of HeLa nuclei phosphoproteome revealed the presence of peptides derived from ITSN1-s, suggesting that ITSN1-s could have access to the nucleus and play a role therein, similarly to other scaffold adaptor proteins [20].

In the present study, we report that a small, but significant fraction of ITSN1-s is present at the steady state in the nucleus of HeLa and HEK 293 cells, where it accumulates on the NE. We show here for the first time that ITSN1-s is able to bind to IMPα and shuttle between the cytoplasm and the nucleus in a CRM-1 dependent fashion. We also identify a bipartite NLS located at residues 1104-1127, capable of conferring energy and Ran dependent nuclear import abilities to a reporter protein.

Experimental

Cell culture and transfections. HeLa, HEK 293-A and HEK 293-T cells were maintained in Dulbecco's modified Eagle's medium (DMEM) supplemented with 10% (v/v) fetal bovine serum (FBS), 50 U/ml penicillin, 50 U/ml streptomycin and 2 mM L-glutamine as described previously [21-23]. For Confocal laser scanning microscopy (CLSM) experiments, 3×10^4 HEK 293-A or 2.5×10^4 HeLa cells were seeded onto polylisinated 12 mm glass coverslips in 24-well plates 1 day before transfection using Lipofectamine 2000 (Thermofisher) according to the manufacturer's recommendations [24]. For live cell imaging experiments, 6×10^5 HeLa cells were seeded in a glass bottom 6-well plate (P06G-0-10F, MatTec) 1 day before transfection using Lipofectamine 3000 (Thermofisher) according to the manufacturer's recommendations. For cytosol/nucleus separation of endogenous and FLAG-ITSN1-s, and for immunoprecipitation between GFP-IMPαΔIBB and FLAG tagged fusion proteins 5 x 10^5 HeLa cells and HEK 293-T cells were seeded in 60 mm diameter dish the day before transfection using Lipofectamine 2000. All experiments were carried out 48 h post transfection.

Plasmid construction. Mammalian expression plasmids were generated using the Gateway™ technology (Invitrogen). ITSN1-s regions of interest were amplified with appropriate primer pairs containing attB sites using plasmid FLAG-ITSN1-s [25] (a kind gift of Peter S. McPherson, McGill University, Montreal, Quebec, Canada) and cloned into plasmid vector pDNR207 (Invitrogen) via BP recombination, to generate entry clones, as previously described [26]. Entry clones were then used to generate C-terminal YFP fusion Mammalian expression vectors following LR recombination reactions with the pDESTnYFP [27] Gateway compatible vector, as described previously [28]. All vectors were confirmed by sequencing. Point mutant derivatives carrying amino acid substitutions of ITSN-NLS (**RKK**NPGGWWEGELQA**RG**KK**R**QIGW-1127, to aatNPGGWWEGELQARGatsQIGW-1127) were generated using appropriate oligo pairs and the Quikchange mutagenesis kit (Agilent technologies) as described previously [29]. As positive and negative controls for response to LMB treatment, plasmids GFP-Rev (2-116), encoding the Rev protein from HIV-1, which shuttles between nucleus and cytoplasm in a CRM-1 dependent manner, and GFP-UL44ΔNLS driving the expression of an exclusively cytosolic version of human cytomegalovirus DNA polymerase processivity factor UL44, were used in addition to the pEGFP-C1 (Clontech) expression vector [30, 31]. Plasmid pEGFP-C1-mIMPαΔIBB, encoding a GFP-tagged deletion mutant of mouse IMPα6 lacking the autoinhibitory IMPβ binding (IBB) domain, therefore binding to cNLSs with high affinity [32], was described elsewhere [33]. pDESTnFLAG-

UL44, a plasmid mediating expression of a FLAG-tagged version of UL44 which is known to be transported into the nucleus by the IMPα/β heterodimer, was used as a positive control in immunoprecipitation experiments with GFP-mIMPαΔIBB [28]. Plasmid pDESTnYFP-NLS[R], encoding a fusion protein between YFP and a minimal cNLS derived from Simian Virus 40 Large Tumor antigen, mediating nuclear targeting via IMPα/β was described elsewhere (Smith et al., unpublished observations).

Confocal laser scanning microscopy (CLSM). HeLa cells were treated as described in [34]. Briefly, cells were washed with PBS, fixed with 4% paraformaldehyde (PFA) for 10 min at room temperature (RT), permeabilized with 0.2% TritonX-100, 2mg/ml BSA, 1mM NaN_3 in PBS on ice three times for 10 min. Cells were subsequently incubated with blocking solution (0.02% TritonX-100, 3% BSA, 1mM NaN_3 in PBS). Primary antibodies α-FLAG (SIGMA), and α-lamin A/C (Thermo fisher) were incubated for 30 min in blocking solution and washed three times for 10 min with wash buffer (PBS 0.02% TritonX-100, 1.5% BSA, 1mM NaN_3). Secondary antibodies (goat α–mouse Cy3, goat α–rabbit Cy2, Jackson Immunoresearch) were incubated for 45 min and washed as described above. Coverslips were mounted using an antifade mounting medium (ProLong Gold-Invitrogen) on a glass slide. CLSM was performed on a ZEISS LSM 510 META confocal laser scanning microscope using the 63X or the 100X Plan-NEOFLUAR oil immersion objective. To analyze the subcellular distribution of spontaneously fluorescent fusion proteins expressed in HEK 293-A cells, cells were transfected and, after 48 h, washed twice in PHEM buffer (60mM PIPES, 25mM HEPES, 10mM EGTA, and 4mM $MgSO_4$) to preserve the cellular cytoskeleton [35], before being fixed with 3% PFA in PHEM buffer for 15 min at RT and mounted onto glass coverslips with FluoromountG (Southern Biotech). Samples were processed by CLSM using a Leica TCT-SP2 system, equipped with a Planapo fluor 63x oil immersion objective (Leica). At least 4 randomly chosen fields were acquired, and a total of at least 30 cells, expressing the fusion proteins of interest to similar levels, were analyzed for each repetition. The Fn/c values were determined using the NIH ImageJ 1.62 public domain software, from single cell measurements for each of the nuclear (Fn) and cytoplasmic (Fc) fluorescence, after the subtraction of fluorescence due to autofluorescence/background [36]. Data was plotted and statistically analyzed using Prism 6 (GraphPad) software.

Live Cell Imaging. HeLa cells were transfected to express the spontaneously fluorescent fusion protein of interest. 48h later, the medium was substituted with complete phenol red free DMEM (A18967, Life Technology). Cells were imaged with a DMi8 inverted microscope (Leica),

equipped with a 40x NA 0.6 objective, a motorized stage and a heated/humidified chamber, at 37°C and 5% CO_2. Several positions have been recorded for each sample. Phase contrast image served as reference for cytoplasm vs. nuclei masking. When required, the Fn/c values relative to each fusion protein were calculated as described above.

Cell treatments. In indicated cases, Leptomycin B (LMB; Sigma L2913; 2.9 ng/ml) was added to cells 8 h before processing samples for imaging, as previously described [37]. Intracellular ATP was depleted by incubating cells for 2h at 37°C in DMEM lacking phenol red and glucose (Thermofisher), supplemented with 10 mmol/L sodium azide and 6 mmol/L 2-deoxy-D-glucose (Sigma), as described previously [38].

Identification of putative NTSs on ITSN1-s. The primary sequences of ITSN1-s (NCBI Accession Number: NP_001001132.1) was scanned for putative NLS and NES using software programs cNLSmapper [38] and NES finder, respectively [39].

Western blot. Samples were heated in reducing SDS sample buffer (80 mM Tris, pH 6.8, 2% SDS, 7.5% glycerol, 0.01% Bromophenol blue) supplemented with 2% 2-mercaptoethanol for 5 min at 95 °C and separated by SDS–PAGE on acrylamide/bisacrylamide gels and analyzed by Western blot (WB) as previously described [21]. Briefly, samples were transferred for 1h onto PVDF membrane, blocked for 1h at 37°C with 5% fat free milk, 0.05% Tween-20 in PBS. PVDF membranes were incubated with specific antibodies: α-ITSN (Abcam), α-FLAG (SIGMA), α-lamin A/C (Thermo fisher), α-ERK 1/2 (Santa Cruz), anti-histone H3 (Santa Cruz), α-tubulin (Santa Cruz), or α-GFP/GST (a generous gift from Prof. Höning, University of Cologne) overnight in PBS Tween 0.05% + 1% fat free milk. The membrane was washed 3 times for 10 min with PBS Tween 0.05% and incubated 1h with one of the following secondary antibodies horseradish peroxidase-conjugated: goat α-mouse and goat α-rabbit (Bethyl), rabbit α-goat (Pierce). Blots were detected using Immobilon Western Classico or Forte (Millipore). Images were acquired using a G:Box Chemi XT Imaging system (Syngene)[40].

Co-immunoprecipitation of protein complexes. HeLa or HEK 293-T cells were washed with PBS 1X and harvested 48 h post transfection as described in [41]. Cells were centrifuged at 800 g for 10 min and pellet was resuspended in ice cold lysis buffer, 50 mM Hepes, 100 mM NaCl, 1% NP-40 + Protease inhibitors cocktail [(PI), 1:1000 (Roche)] for 10 min on ice. Cells were then sonicated at

15% of instrument power (Sonopuls, Bandelin) for 10 sec. After clarification, supernatants were incubated with 4 µg of the α–ITSN, α–Lamin, α-FLAG antibodies or without antibody as negative control as indicated, overnight at 4 °C, with gentle rocking. The following day, 50 µL of protein A/G beads (Santa Cruz Biotechnology) were added and the mixtures incubated for 4 h. After 3 washes with PBS 1X, beads were resuspended in SDS sample buffer for 5 min at 95 °C and centrifuged at 800 g for 3 min before the supernatant were collected. For immunoprecipitation of GFP-mIMPaDIBB in the presence of FLAG-ITSN1-s or not, the protocol has been adapted from [42]. HEK 293-T cells were washed with PBS 1X and harvested 48 h post transfection. Cells were centrifuged at 800 g for 10 min and pellet was resuspended in ice cold lysis buffer, 50 mM Hepes, 100 mM NaCl, 1mM $MgCl_2$, 1% NP-40 + Protease inhibitors cocktail [(PI), 1:1000 (Roche)] for 10 min on ice. Cells were then sonicated as described above. After clarification, supernatants were incubated with 4 µg of the α-FLAG as indicated, overnight at 4 °C, with gentle rocking. The following day, 50 µL of protein A/G beads were added and the mixtures incubated for 4 h. After 3 washes with 50 mM Hepes, 100 mM NaCl, 1mM $MgCl_2$, 1% NP-40, beads were resuspended in SDS sample buffer and treated as described above. Samples were subjected to SDS-PAGE/WB analysis.

Subcellular fractionation. In order to separate nuclei from cytoplasm a protocol from Nabbi et al. has been adapted [43]. Briefly, HeLa cells grown to 90% confluency in 10 cm dishes were washed with ice cold PBS and scraped. Cells were centrifuged at 10000 g for 10 sec. Cell pellets were resuspended in PBS with 0.1% NP-40 and triturated with a P1000 micropipette. The lysed cells suspension was centrifuged at 10000 g for 10 sec. The supernatant representing the cytoplasmic fraction was isolated, the nuclei were gently resuspended in PBS with 0.1% NP-40 and centrifuged again. Nuclear pellet was resuspended in SDS sample buffer and sonicated twice at 15% of instrument power (Sonopuls, Bandelin) for 6 sec on ice. Fractions were analyzed by SDS-PAGE/WB as described above.

Nucleoplasm/Nuclear envelope separation. To separate nucleoplasm and nuclear envelope, nuclei obtained as described above were resuspended in NP-40 buffer (PBS 0.5X, 10 mM $MgCl_2$, 50 mM MOPS pH 7.4, 0.5% NP-40, DNAase 5 U/mL, PI 1:1000, and incubated on ice 5 min. Samples were centrifuged at 20000 g for 10 min and supernatants were collected and considered as nucleosol. Pellet (nuclear envelope) were resuspended in RIPA buffer (150 mM NaCl, 1% NP-40, 50 mM Tris-HCl pH 8, 0.1% SDS, 0.5% Sodium desossicolate, PI) and tip-sonicated 12 sec at 15%

of instrument power (Sonopuls, Bandelin). Fractions were analyzed by SDS-PAGE/WB as described above.

Chemical crosslinking to detect DNA-binding proteins. In order to visualize if ITSN1-s is a DNA binding protein a protocol from Qiu et al [44] has been adapted. HeLa cells (10 cm dish, 90% confluency) were trypsinized and collected by centrifugation at 300 g for 5 min at 4 °C. Cells were washed with ice-cold PBS to remove culture medium and FBS. *In vivo* cross-linking was achieved by adding PFA to 1 mL of cell suspension in PBS to obtain a final concentration of 1% (w/v). After incubating at RT, PFA was quenched by glycine to a final concentration of 125 mM and incubated at RT for 5 min. The cross-linked cells were collected by centrifugation (300 g at 4 °C for 5 min), and the cell pellet was washed twice with cold PBS. Nuclei isolation was carried out using a protocol adapted from that reported by Henrich et al. [45, 46]. The cross-linked HeLa cell pellet (2x 10 cm dishes, 70% confluent) was resuspended in 10 volumes of ice-cold hypotonic lysis buffer A containing 10 mM HEPES (pH 7.4), 10 mM KCl, 1.5 mM $MgCl_2$, 1 mM DTT, and PI 1:1000. After incubation on ice for 30 min, 0.5% (v/v) NP-40 was added to the lysis buffer. Cells were then gently lysed with a Dounce homogenizer and the nuclear fraction was collected by centrifugation. The nuclear fraction resuspended in buffer B (250 mM sucrose, 10 mM $MgCl_2$, 20 mM Tris-HCl (pH 7.4) and 1 mM DTT) was layered over a two-step sucrose gradient cushion [1.3 M sucrose, 6.25 mM $MgCl_2$, 20 mM Tris-HCl (pH 7.4), 0.5 mM DTT above 2.3 M sucrose in 2.5 mM $MgCl_2$ and 20 mM Tris-HCl (pH 7.4)] and centrifuged subsequently at 19000g at 4 °C for 45 min. The isolated nuclei were washed with buffer A and collected by centrifugation at 1000g.
Isolation of DNA-Protein Complexes, cross-Linking Reversal and DNA Removal were performed as described previously [44]. The purified DNA-binding proteins were separated using a NuPage 4-12% Bis-Tris protein gel (Invitrogen).

Statistical analysis. Statistically significant differences between datasets were determined with Student's *t*-Test (Graphpad software, Inc.). P values of less than 0.05 were considered statistically significant with $*p \leq 0.05$, $** p \leq 0.01$, $*** p \leq 0.001$. Values shown are the mean ± standard error of the mean (SEM) relative to at least three independent experiments [47, 48].

Results

A fraction of ITSN1-s localizes to the nucleus

In order to investigate ITSN1-s subcellular localization, HeLa cells were transfected with a FLAG-ITSN1-s expression plasmid and subjected to biochemical separation of nuclear and cytosolic fractions. Mock-transfected cells were used as a negative control. Then, ITSN1-s distribution was analyzed in the two fractions by SDS-PAGE/WB. ERK1/2 and lamin A/C were used as reference proteins for cytosolic and nuclear compartments, respectively. Both FLAG-tagged and endogenous ITSN1-s were enriched in the cytosol, but detectable in both fractions, while reference proteins were localized exclusively in the specific fraction, proof of a clean compartment separation (Fig. 1A). We also confirmed our results by immunofluorescence (IF), limiting our analysis to FLAG-ITSN1-s due to the lack of suitable commercial antibodies. The protein presented mainly a cytoplasmic localization, although it was also visible in the cell nucleus (Fig. 1B). Thus, our data demonstrate the existence of a nuclear pool of ITSN1-s.

ITSN1-s is enriched in the nuclear envelope

The relative amount of nuclear FLAG-ITSN1-s detectable in the nucleus after subcellular fractionation appears higher than that observable by IF (Fig. 1), raising the possibility that the majority of nuclear FLAG-ITSN1-s is associated to the nuclear envelope (NE) rather than in the nucleoplasm. To verify this hypothesis, nucleoplasmic and NE fractions from purified nuclei of HeLa cells transfected to express FLAG-ITSN1-s were analyzed by SDS-PAGE/WB to detect the cytosolic marker ERK1/2, the NE marker lamin A/C, as well as FLAG-ITSN1-s. As expected, while ERK1/2 was not detectable in the nuclear fraction, lamin A/C localized exclusively in the NE fraction (Fig. 2A). FLAG-ITSN1-s was both detectable in the nucleoplasmic and the NE fractions, but highly enriched in the latter, consistent with the idea that ITSN1-s could associate with the NE. IF analysis revealed that FLAG-ITSN1-s partially colocalizes with lamin A/C on the NE (Fig. 2B). Subsequently, we investigated the interaction between ITSN1-s and lamin A/C by co-immunoprecipitation (co-IP) analysis. HeLa cells were lysed, and ITSN1-s complexes pulled down using either an α-ITSN or an α-lamin A/C antibody. SDS-PAGE/WB analysis revealed the presence of two bands corresponding to lamin A and C in the ITSN1-s pull down lane and of a ITSN1-s band in the lamin A/C pull down (Fig. 2C).

Finally, since some endocytic proteins were found to be part of transcription complexes [49], we tested the possibility that ITSN1-s could bind DNA. To this end, we adapted a protocol which includes chemical cross-linking of cells followed by nuclei isolation and purification of covalently

bound DNA-protein complexes [44]. DNA protein complexes were isolated and analyzed by a SDS-PAGE/WB using α-ITSN1, in addition to α-tubulin and α-Histone H3 antibodies as negative and positive controls, respectively [50]. As expected, Histone H3 was detectable in the DNA protein complexes lane (DPC) as well as in the cell homogenate (H), whereas tubulin, which is incapable of binding to DNA, was detectable only in the cell homogenate (Fig. 2D). Importantly FLAG-ITSN1-s could not be detected in the DPC, suggesting that ITSN1-s does not interact with cellular DNA. Taken together our results indicate that a small, but detectable amount of ITSN1-s localizes within the cell nucleus at the steady state, where it preferentially associates with the NE, possibly interacting with lamin A/C.

ITSN1-s interacts with IMPα

The fact that a certain fraction of the 145 kDa protein ITSN1-s can gain access to the nucleus implies the protein is actively translocated into the nucleus in a NLS-dependent fashion by IMPs. A bioinformatics analysis using the NLS prediction software "cNLS MAPPER" revealed the presence of a putative bipartite cNLS (**RKK**NPGGWWEGELQA**R**G**KKR**QIGW-1127), located in the C-terminal, SH3 portion of ITSN1-s (Fig. 3A,B). Such sequence strongly resembles the prototype bipartite cNLS originally described on nucleoplasmin (**KR**PAAT**KK**AGQA**KKKK**-170) and perfectly matches the consensus for such signals. This finding raised the possibility that ITSN1-s could bind to the IMPα/β heterodimer. To assess this hypothesis by co-IP experiments, HEK 293-T cells were transfected to express GFP-IMPαΔIBB either individually or in the presence of FLAG-ITSN1-s. The former is a GFP-tagged derivative of IMPα that lacks the autoinhibitory IMPβ binding (IBB) domain, and that therefore binds to NLSs with an affinity comparable to that of the IMPα/β heterodimer [32]. As a positive control, GFP-IMPαΔIBB was also expressed in the presence of FLAG-UL44, a protein known to be recognized by the IMPα/β heterodimer [28]. Proteins were subsequently immunoprecipitated in the presence or in the absence of the FLAG antibody. As expected, FLAG-UL44 could be co-immunoprecipitated with GFP-IMPαΔIBB, whereas no GFP-IMPαΔIBB was obtained after incubation of cell lysates in the absence of the αFLAG antibody, indicating that GFP-IMPαΔIBB did not interact unspecifically with protein A/G beads (Fig. 4A). Importantly, GFP-IMPαΔIBB could be also co-immunoprecipitated by the α–FLAG antibody from cells co-expressing FLAG-ITSN1-s, but not from cells expressing GFP-IMPαΔIBB alone, indicating that GFP-IMPαΔIBB did not interact unspecifically with the α–FLAG antibody (Fig. 4B). Taken together these results show that ITSN1-s is able to interact with IMPα, thus being actively transported into the nucleus.

ITSN1-s is a nucleocytoplasmic trafficking protein

Despite its ability to bind to IMPα, at the steady state ITSN1-s preferentially localizes in the cytosol. It is therefore possible that, as described for other endocytic proteins [6], ITSN1-s shuttles between the nucleus and the cytoplasm thanks to the simultaneous presence of NLS and NES. A bioinformatics analysis using the NES prediction software "NES finder", integrated by visual inspection based on a systematic analysis of NES consensus performed in eukaryotic cells [10], identified 6 putative hydrophobic rich NESs [NES A-F] distributed throughout the 3 regions of ITSN1-s (EH-like homology; EHs, aas 1-380; coiled coil; CC, aas 381-680 and; SH3s, aas 681-1220) (Fig. 3A,B). The presence of putative hydrophobic NESs within ITSN1-s indeed suggested that the protein could undergo nucleocytoplasmic shuttling in a CRM-1 dependent manner.

In order to confirm this hypothesis, the subcellular localization of ITSN1-s was tested in HeLa cells upon LMB-mediated inhibition of CRM1 activity. FLAG-ITSN1-s transiently transfected cells were treated or not with LMB, before CLSM analysis to quantify their levels of nuclear accumulation. In addition to FLAG-ITSN1-s, cells were also transfected with GFP, GFP-Rev, a protein known to accumulate in the nucleus after LMB treatment, as well as with GFP-UL44ΔNLS, a ≈ 180 kDa dimeric cytosolic protein which is excluded from the nucleus due to the lack of a functional NLS. Addition of LMB did not affect the subcellular localization of either GFP and GFP-UL44ΔNLS, implying the treatment did not affect cell viability and morphology as well as NPC permeability, while it caused GFP-Rev to strongly accumulate in the cell nucleus (Fig. S1 and Table S1). Importantly, after treatment with LMB, FLAG-ITSN1-s nuclear staining became significantly more evident (Fn/c from 0.15 to 0.45), although the protein did not accumulate in the cell nucleus to high levels (Fig. 5A,B and Table S2). Thus, ITSN1-s can shuttle between the nucleus and the cytosol in a IMPα/β and CRM1-dependent fashion.

ITSN1-s CC and SH3 regions can independently undergo nucleocytoplasmic shuttling.

In an effort to identify ITSN1-s functional NTSs among the putative ones predicted, we generated several ITSN1-s deletion mutants fused to the C-terminus of YFP. We initially verified that addition of a YFP-tag did not interfere with ITSN1-s subcellular localization and nucleocytoplasmic shuttling abilities. To this end, HeLa cells were transfected to express YFP-ITSN1-s, whose subcellular localization was initially monitored by live cell imaging every min for a period of 30 min. As expected, YFP-ITSN1-s localized mainly in the cytoplasm, with evident dots reminiscent of endocytic vesicles, which appeared to be highly mobile (Fig. S2 and Mov. S1).

In a second series of experiments, HeLa cells were transfected to express either YFP-ITSN1-s or

GFP-UL44ΔNLS, treated with either LMB or with solvent, and the subcellular localization of the fusion protein of interest visualized every 15 min for 10 h. As expected, YFP-ITSN1-s gradually accumulated into the nucleus, reaching a maximum approximately 5 h after LMB addition, whereas the negative control GFP-UL44ΔNLS remained mainly cytosolic for the whole duration of the experiment (Fig. S3 and Mov. S2). Therefore, YFP-ITSN1-s could be used to study the nucleocytoplasmic properties of ITSN1-s. Beside full length ITSN1-s (1-1220), we generated plasmids mediating the expression of five additional deletion mutants: YFP-ITSN1-s-ΔEHs (316-1220), lacking the N-terminal epsin like domain; YFP-ITSN1-s-ΔSH3s (1-680), lacking the C-terminal SH3 domains; YFP-ITSN1-s-SH3s (681-1220); YFP-ITSN1-s-EHs (1-315) and YFP-ITSN1-s-CC (316-680) (Fig. 6A). As a first step towards the characterization of such variants, their molecular weights were verified by SDS-PAGE/WB using an α-GFP antibody (Fig. 6B). Fusion proteins migrated at the expected molecular weights (YFP-ITSN1-s: 160 kDa, YFP-ITSN1-s-ΔEHs: 125kDa, YFP- ITSN1-s-ΔSH3s: 101 kDa, YFP-ITSN1-s-SH3s: 85 kDa, YFP-ITSN1-s-EHs: 61 kDa, YFP-ITSN1-s-CC: 66 kDa). Multiple bands of higher molecular weight could be detected for the YFP-ITSN1-s-CC fusion, most likely due to protein multimerization/aggregation. Secondly, we decided to investigate their subcellular localization either in the absence or in the presence of LMB. HEK 293-A cells were transiently transfected with appropriate expressing vectors and the subcellular localization of YFP-ITSN1-s was compared by quantitative CLSM to that of the above described deletion mutants. Along with YFP-ITSN1-s fusions, the previously described controls (GFP, GFP-Rev and GFP-UL44ΔNLS) were used to verify the functionality of LMB treatment (Fig. 6C). As expected, GFP evenly distributed between nucleus and cytoplasm both in absence and presence of LMB (Fn/c 1.27 $\pm$ 0.14 *vs* 1.50 + 0.28). Similarly, GFP-UL44ΔNLS, having a molecular weight a ≈ 180 kDa, was retained in the cytosol in both cases (Fn/c 0.10 + 0.09 vs 0.17 $\pm$ 0.08). Importantly, LMB addition significantly enhanced nuclear accumulation of GFP-Rev (Fn/c 0.16 $\pm$ 0.03 vs 16.97 $\pm$ 9.87), which strongly accumulated in the nucleoli. Taken together, our data indicate that LMB treatment functionally inhibited CRM-1 mediated nuclear export without affecting NE permeability (see Fig. 6C,D, *left* panel and Table S3). As expected, in the absence of LMB, YFP-ITSN1-s mainly localized in the cytoplasm of untreated cells (Fig. 6C and Fig. 2D, right panels and Table S4; Fn/c 0.11 ± 0.08) with a punctuate pattern present in the cytoplasm and in close proximity to the plasma membrane, thus resembling that of endocytic vesicles. Deletion of EH domains (YFP-ITSN1-s-ΔEH) altered ITSN1-s localization pattern, in that the punctuate structures observed for FL-ITSN1-s were not detectable, and large protein aggregates were often present in strongly expressing cells. However, the protein was still mainly detectable in the cytoplasm (Fn/c 0.07 $\pm$ 0.04). Removal of both EH

and CC regions (YFP-ITSN1-s-SH3s), caused the protein to localize in the cytosol with a mainly diffuse pattern, although a few vesicle-like dots were still detectable (Fn/c 0.10 ± 0.04). On the contrary, removal of ITSN1-s SH3 region (YFP-ITSN1-s-ΔSH3s) did not change the punctate pattern described for ITSN1-s but caused a significant increase of nuclear signal (Fn/c 0.42 ± 0.09). When both the CC and SH3 regions were simultaneously deleted (YFP-ITSN1-s-EHs), the subcellular localization was completely altered: this protein equally distributed between the nucleus and the cytoplasm with a diffuse pattern (Fn/c 1.13 ± 0.35). In addition, vesicle-like dots or protein aggregates were not detectable. Finally, YFP-ITSN1-s-CC fusion, devoid of both EH and SH3 regions, localized mainly in the cytoplasm, but entered the nucleus slightly more efficiently with respect to YFP-ITSN1-s (Fn/c 0.24 ± 0.08). The protein distributed with a diffuse pattern in the cytoplasm, with the presence of large protein aggregates in the cytosolic compartment of highly expressing cells.

Importantly, addition of LMB increased nuclear levels of YFP-ITSN1-s (Fn/c 0.11 ± 0.08 vs 0.41 ± 0.11), as well as of all YFP-ITSN1-s deletion mutants, apart from YFP-ITSN1-s-EHs (Fn/c 1.13 ± 0.35 vs 1.34 ± 0.32, see Fig. 6C,D). Indeed, both ITSN1-s-CC and ITSN1-s-SH3 responded to LMB treatment (Fn/c of 0.24 vs. 0.72 and 0.10 vs 0.78, respectively) similarly to ITSN1-s-ΔEH and ITSN1-s-ΔSH3 (Fn/c of 0.07 vs. 0.32 and 0.42 vs 1.32, respectively). Therefore, both ITSN1-s CC and SH3 regions were sufficient to confer LMB-dependent nucleocytoplasmic shuttling properties to YFP. Taken together, the subcellular localization of ITSN1-s and its deletion mutants at the steady state suggest that the N-terminal EH domain (to a larger extent) and the C-terminally located SH3 regions play a role in ITSN1-s localization to endocytic vesicles-like dots, while the CC domain can cause protein aggregation, when expressed outside the physiological context of FL-ITSN1-s. In addition, LMB experiments suggest that ITSN1-s could contain multiple NTSs located in the CC and SH3 regions, whereas ITSN-EH domain does not actively contribute to the protein's nucleocytoplasmic shuttling ability, and NESs [A-C] are not functional in terms of mediating CRM-1 dependent nuclear export.

ITSN1-s residues 1104-1127 represent a functional cNLS. As a first attempt towards the characterization of ITSN1-s nucleo-cytoplasmic shuttling process, we decided to identify its NLS. Our bioinformatics analysis could not detect any cNLS in ITSN1-s-CC region, but revealed the presence of a putative bipartite cNLS in the SH3 region, within ITSN1-s-SH3D domain (**RKK**NPGGWWEGELQA**R**G**KKR**QIGW-1127) (Fig. 3). To validate its functionality, we generated an expression plasmid encoding such sequence C-terminally fused to YFP (YFP-ITSN1-s-NLS) and analyzed the ability of the YFP-ITSN1-s-NLS fusion protein to accumulate in

the nucleus in an energy-dependent manner. We also analyzed the subcellular localization of YFP alone or of the control YFP-NLS[R] fusion protein, known to localize to the cell nucleus through interaction with the IMPα/β heterodimer (Smith et al., unpublished observations). As expected, when cells were maintained in normal media, YFP-NLS[R] accumulated into the nucleus of transfected cells (Fn/c 2.8) in significantly higher levels than YFP alone (Fn/c 1.1; Fig. 7 and Table S5). Depletion of intracellular ATP significantly decreased the nuclear accumulation of YFP-NLS[R], without affecting the subcellular localization of YFP alone (Fn/c of 1.5 and 1.1 respectively; Fig. 7). Importantly, YFP-ITSN1-s-NLS accumulated into the nucleus at significantly higher levels as compared to YFP alone when cells were maintained in normal media (Fn/c 1.8), and its nuclear accumulation was significantly impaired after incubation in the energy depletion media (Fn/c 1.3). These data clearly show that ITSN1-s residues 1104-1127 represent a basic NLS capable of conferring energy dependent nuclear localization to heterologous proteins.

ITSN-NLS is essential for nuclear targeting of ITSN1-s C-terminal domain. We decided to test the impact of ITSN1-s-NLS on nuclear targeting of the protein. We compared the subcellular localization of YFP-ITSN1-s to that of its derivative YFP-ITSN1-sΔNLS, where basic residues of its NLS (**RKK**NPGGWWEGELQA**R**G**KKR**QIGW-1127) were substituted with hydrophobic ones (ΔNLS; aatNPGGWWEGELQA**R**GatsQIGW-1127; see Fig. 8A), either in the absence or in the presence of LMB. Under both conditions, the NLS defective derivative localized with a very similar pattern as compared to the wild-type protein (Fig. 8B). This was not surprising, since deletion of the whole ITSN1-s-SH3 region, comprising ITSN1-s-NLS, did not impair the ability of the protein to enter the nucleus upon LMB treatment, implying a contribution of ITSN1-s-CC region in nucleocytoplasmic shuttling of ITSN1-s (Fig. 6). In order to study the contribution of ITSN1-s-NLS to nuclear import of the protein independently of the contribution of ITSN1-s-CC region, we analyzed the subcellular localization of a series of ITSN1-s C-terminal domain deletions, including YFP-ITSN1-s-SH3s, encompassing residues 681-1220; YFP-ITSN1-s-SH3(A-D) comprising residues 681-1173; and YFP-ITSN1-s-SH3(D-E) comprising ITSN1-s residues 1074-1220, either carrying the wild-type or the mutated NLS (Fig. 8). In the absence of LMB both YFP-ITSN1-s-SH3 and YFP-ITSN1-s-SH3(A-D) localized mainly in the cytosol, and inactivation of ITSN-NLS did not affect the proteins subcellular localization (Fn/c c. 0.2, see Fig. 8). Upon LMB treatment, both YFP-ITSN1-s-SH3 and YFP-ITSN1-s-SH3(A-D) significantly accumulated into the nucleus (Fn/c of c. 0.8 and 1.1, respectively), while their NLS mutated counterparts were mainly retained in the cytosol (Fn/c of c. 0.4), clearly showing the importance of ITSN1-s residues 1104-1127 for nuclear targeting. The contribution of ITSN1-s-NLS to nuclear import was even more evident when

484 analyzing the subcellular localization of YFP-ITSN1-s-SH3(D-E). In absence of LMB, this protein
485 was detectable in the nucleus, compatible with its ability to passively enter the nucleus by passive
486 diffusion (Fn/c 0.9), while addition of LMB increased its nuclear accumulation (Fn/c 1.5).
487 Importantly, in the absence of LMB, YFP-ITSN1-s-SH3(D-E)ΔNLS localized to the nucleus to
488 lower levels (Fn/c of 0.5) as compared to its NLS bearing counterpart, further confirming the
489 importance of ITSN1-s-NLS in nuclear import of the protein (Fig. 8B,C and Table S6). Overall our
490 data also suggest that ITSN1-s-NESE -located within SH3D domain - is the functional NES within
491 the SH3 region, while NESF - located within SH3E domain- does not contribute to CRM-1 nuclear
492 export. Indeed, both YFP-ITSN1-s-SH(A-D) and YFP-ITSN1-s-SH3(D-E), accumulate to the
493 nucleus in the presence of LMB. Furthermore, site specific mutagenesis for NESF did not abolish
494 LMB responsiveness, nor increased steady state nuclear localization either in the SH3(A-E) or
495 SH3(D-E) context (data not shown). However, attempts to mutate NESE hydrophobic residues
496 resulted in increased nuclear accumulation in the presence of LMB (data not shown), probably by
497 interfering with the nearby-located NLS, thus precluding formal proof that NESE is a functional
498 NES.
499
500 **ITSN1s-CC shuttles between the nucleus and the cytoplasm independently of the presence of**
501 **putative NTSs**. Our data indicate that ITSN1-s-CC is capable of nucleocytoplasmic shuttling.
502 However, no evident NTSs are present within its sequence, with the exclusion of a stretch of aa
503 containing four L residues, which could resemble the NES originally described on HIV-1 Rev
504 (NESD: LELEKQLEKQRELL-419, see Fig. 3). Since NESD is located at the N-terminal portion of
505 the CC region, we decided to test its functionality by analyzing the subcellular localization of the N-
506 terminal (residues 316-456, containing NESD) and of the C-terminal (residues 457-680) portions of
507 ITSN1-s CC region, either in the absence or in the presence of LMB (Fig. 9A,B,C and Table S7).
508 Strikingly, in the absence of LMB both YFP-ITSN1-s(316-456) and YFP-ITSN1-s(457-680) mainly
509 localized in the cytosol of transfected cells, (Fn/c of 0.7 and 0.3, respectively) but accumulated in
510 the nucleus upon LMB treatment (Fn/c of 1.4 and 1.2, respectively). Surprisingly, mutation of
511 ITSN1-s-NESD hydrophobic residues (LELEKQLEKQREL-419 to qEaEKQqEKQREL-419), did
512 not affect protein subcellular localization either in the absence or in the presence of LMB.
513 Therefore, ITSN1-s-CC appears capable of shuttling between nucleus and cytosol in the absence of
514 evident NTSs.
515
516
517 **Discussion**
518

519 In the present work we showed for the first time that the adaptor scaffold protein ITSN1-s, known
520 to be involved in several signaling and endocytic processes [1, 13, 51], and interacting with a
521 plethora of factors involved in endocytosis, cytoskeleton rearrangements, cell signaling and survival
522 [52-54], is a nucleocytoplasmic shuttling protein, which accumulates in the cell nucleus upon
523 pharmacological ablation of CRM1-dependent nuclear export. At the steady state, a fraction of
524 ITSN1-s localizes at the nucleus and is enriched at the nuclear envelope, where it interacts with
525 lamin A/C.
526 The identification of ITSN1-s nucleocytoplasmic shuttling sequences has been hampered by the
527 evidence that both ITSN1-s CC and SH3 regions can shuttle between nucleus and cytosol
528 independently of each other (Fig. 6). Moreover, the ITSN-1s CC region is apparently devoid of
529 evident NTSs, bearing no putative cNLSs and only one putative leucine-rich NES (NESD:
530 LELEKQLEKQRELL-419), whose mutation to qEaEKQqEKQRELL-419 did not affect LMB
531 responsiveness (Fig. 9). Therefore, it is not known how ITSN-1s CC could undergo cytoplasmic
532 shuttling. One possibility is that the α-helix rich CC domain can interact with the FG repeats of the
533 NPC to allow passage in and out of the nucleus, in analogous fashion as it has been demonstrated
534 for HEAT repeats containing proteins such as IMPβ [55]. Another possibility is that one of the
535 several cellular proteins capable of interacting with ITSN1-s-CC region, is responsible for transport
536 across the NPCs through a "piggy-back" mechanism. Such proteins include the nucleocytoplasmic
537 shuttling Eps15 and HIP1 proteins, as well as endogenous ITSN1-s, ITSN1-L and ITSN2-s [16, 17,
538 56-58]. Despite the confounding effect due to the presence of the CC-region, we were able to
539 clearly demonstrate the existence of a functional bipartite cNLS in the SH3 region of ITSN1-s
540 (ITSN1-s-NLS: **RKK**NPGGWWEGELQA**R**G**KKR**QIGW-1127). ITSN1-s-NLS is capable of
541 conferring ATP dependent nuclear targeting to YFP (Fig.7), and mutation of its basic residues
542 impairs nuclear targeting of several YFP-ITSN1-s SH3 deletion mutants in the presence of LMB
543 (Fig. 8). However, mutation of ITSN1-s-NLS in the context of the full length protein does not
544 abolish its ability to enter the nucleus, most likely due to the fact that the CC region can mediate
545 nuclear import and that deletion of the SH3 region of ITSN1-s similarly does not abolish the
546 protein's nucleocytoplasmic shuttling properties (see Fig. 6). The bipartite nature of the ITSN1-s-
547 NLS was confirmed by CLSM quantitative analysis showing that deletion of upstream basic cluster
548 alone only partially affected nuclear accumulation as compared to mutation of both clusters, in the
549 context of the YFP-ITSN1-s-SH3(D-E) fusion protein (not shown), implying that both basic
550 stretches of aa are required for optimal NLS activity [59].
551 Similarly to ITSN1-s, several endocytic adaptor proteins undergo nucleocytoplasmic
552 trafficking, mainly to perform additional, specialized tasks within the nucleus, thus being dubbed

"moonlighting" proteins [56, 60-62]. A number of moonlighting proteins, such as Paxilin and EHD2 migrate to the nucleus to regulate cellular proliferation and transcription processes [63, 64]. Our data, showing that ITSN1-s concentrates on the NE, where it interacts with lamin A/C (Fig. 2A-C), and does not bind to cellular DNA (Fig. 2D), rather suggest the possibility that ITSN1-s might play a role at the NE. It has been recently shown that a fourth endosomal route, besides recycling endosomes, endolysosomes or Golgi apparatus, transports cell surface receptors to the nucleoplasm through docking and membrane fusion of a population of endosomes with the nuclear envelope [65]. Such Nuclear Envelope Associated Endosomes (NAE) route may be an alternative mechanism by which external stimuli can influence cellular activity independently of the conventional signaling cascades that operate in the cytosol, and ITSN1-s could therefore be a new player in such route, helping to transport molecules from the plasma membrane to the nucleoplasm, as it has been hypothesized for Epidermal Growth Factor Receptor. It is very likely that this process comprises a series of tightly regulated events, hence experiments to unravel the mechanisms regulating ITSN1-s shuttling to the nucleus are undergoing in our laboratories. Furthermore, we do not exclude that the process of nuclear localization might be dependent on cell cycle phase, as it happens for other proteins [6, 66-68].

Since modifications of the endocytic process have been recently linked to malignancy [69, 70], it is likely that rerouting of endocytic proteins to other pathways or compartments due to moonlighting functions could be functionally linked to tumorigenesis. In this context, a very recent study showed that APPL1 and APPL2, Rab5 effector proteins and multifunctional adaptors containing different domains, implicated in several signaling pathways, and recently discovered as nucleocytoplasmic shuttling proteins [49], are required for the nuclear translocation of type I serine/threonine kinase receptors intracellular domain (TβRI-ICD), thereby promoting progression of prostate cancer cells [71]. Our results might have important implications for the process of carcinogenesis. ITSN1-s is highly expressed in pancreatic, lung, liposarcomas and Wilm's tumors, as shown in ONCOMINE database. Furthermore, ITSN1-s is necessary for malignant glioma cell proliferation and for *in vitro* and *in vivo* tumorigenic properties of primary human neuroblastoma tumors [72, 73]. It is evident that ITSN1-s plays a critical role in this process due to its tertiary structure, allowing its domains to make contacts with many specific targets. Furthermore, its role in tumorigenesis has been linked to signaling regulation rather than endocytosis although the signaling pathways involved have only been started to be unveiled.

In conclusion, our results suggest a new scenario that foresees the nucleocytoplasmic shuttling of ITSN1-s as an important clue for understanding the physiological and disease-related role of this scaffold protein.

Acknowledgements

We thank Peter Mc.Pherson (McGill University, Montreal, Quebec, Canada) for sharing pRK1S plasmid and Stephan Höning (University of Cologne, Germany) for sharing the rabbit α-GFP/GST antibody.

Funding information

This work was supported by University of Brescia Research fund (ex 60%) to AR, DR and LC, and by University of Padua grant 60A07-1024/15 to Gualtiero Alvisi.

Conflict of interest

The authors declare that they have no conflict of interest.

Author contribution statement

AR and DR conceived the project. AR and GA designed the experiments. AR, GA, LP, NM, AC, AC, VdA, CZ, MT performed the experiments. AR, GA and LP wrote the paper. All authors analyzed the data and proofread the paper prior to submission.

References

1 Langeberg, L. K. and Scott, J. D. (2015) Signalling scaffolds and local organization of cellular behaviour. Nat Rev Mol Cell Biol. **16**, 232-244

2 Buday, L. and Tompa, P. (2010) Functional classification of scaffold proteins and related molecules. FEBS J. **277**, 4348-4355

3 Adams, S. J., Aydin, I. T. and Celebi, J. T. (2012) GAB2--a scaffolding protein in cancer. Mol Cancer Res. **10**, 1265-1270

4 Ravichandran, K. S. (2001) Signaling via Shc family adapter proteins. Oncogene. **20**, 6322-6330

5 Borlido, J., Zecchini, V. and Mills, I. G. (2009) Nuclear trafficking and functions of endocytic proteins implicated in oncogenesis. Traffic. **10**, 1209-1220

6 Pyrzynska, B., Pilecka, I. and Miaczynska, M. (2009) Endocytic proteins in the regulation of nuclear signaling, transcription and tumorigenesis. Molecular oncology. **3**, 321-338

7 Beaulieu, J. M. and Caron, M. G. (2005) Beta-arrestin goes nuclear. Cell. **123**, 755-757

8 Tran, E. J., Bolger, T. A. and Wente, S. R. (2007) SnapShot: nuclear transport. Cell. **131**, 420

9 Kobe, B. (1999) Autoinhibition by an internal nuclear localization signal revealed by the crystal structure of mammalian importin alpha. Nat Struct Biol. **6**, 388-397

10 Kosugi, S., Hasebe, M., Tomita, M. and Yanagawa, H. (2008) Nuclear export signal consensus sequences defined using a localization-based yeast selection system. Traffic. **9**, 2053-2062

11 Fung, H. Y. and Chook, Y. M. (2014) Atomic basis of CRM1-cargo recognition, release and inhibition. Semin Cancer Biol. **27**, 52-61

12 Tsyba, L., Nikolaienko, O., Dergai, O., Dergai, M., Novokhatska, O., Skrypkina, I. and Rynditch, A. (2011) Intersectin multidomain adaptor proteins: regulation of functional diversity. Gene. **473**, 67-75

13 Dergai, O., Dergai, M., Skrypkina, I., Matskova, L., Tsyba, L., Gudkova, D. and Rynditch, A. (2013) The LMP2A protein of Epstein-Barr virus regulates phosphorylation of ITSN1 and Shb adaptors by tyrosine kinases. Cellular signalling. **25**, 33-40

14 Yamabhai, M., Hoffman, N. G., Hardison, N. L., McPherson, P. S., Castagnoli, L., Cesareni, G. and Kay, B. K. (1998) Intersectin, a novel adaptor protein with two Eps15 homology and five Src homology 3 domains. The Journal of biological chemistry. **273**, 31401-31407

15 Hunter, M. P., Russo, A. and O'Bryan, J. P. (2013) Emerging Roles for Intersectin (ITSN) in Regulating Signaling and Disease Pathways. International journal of molecular sciences. **14**, 7829-7852

16 Sengar, A. S., Wang, W., Bishay, J., Cohen, S. and Egan, S. E. (1999) The EH and SH3 domain Ese proteins regulate endocytosis by linking to dynamin and Eps15. The EMBO journal. **18**, 1159-1171
17 Wong, K. A., Wilson, J., Russo, A., Wang, L., Okur, M. N., Wang, X., Martin, N. P., Scappini, E., Carnegie, G. K. and O'Bryan, J. P. (2012) Intersectin (ITSN) family of scaffolds function as molecular hubs in protein interaction networks. PloS one. **7**, e36023
18 Gerth, F., Japel, M., Pechstein, A., Kochlamazashvili, G., Lehmann, M., Puchkov, D., Onofri, F., Benfenati, F., Nikonenko, A. G., Fredrich, K., Shupliakov, O., Maritzen, T., Freund, C. and Haucke, V. (2017) Correction for Gerth et al., Intersectin associates with synapsin and regulates its nanoscale localization and function. Proceedings of the National Academy of Sciences of the United States of America. **114**, E11060
19 Pechstein, A., Gerth, F., Milosevic, I., Japel, M., Eichhorn-Grunig, M., Vorontsova, O., Bacetic, J., Maritzen, T., Shupliakov, O., Freund, C. and Haucke, V. (2014) Vesicle uncoating regulated by SH3-SH3 domain-mediated complex formation between endophilin and intersectin at synapses. EMBO reports
20 Beausoleil, S. A., Jedrychowski, M., Schwartz, D., Elias, J. E., Villen, J., Li, J., Cohn, M. A., Cantley, L. C. and Gygi, S. P. (2004) Large-scale characterization of HeLa cell nuclear phosphoproteins. Proceedings of the National Academy of Sciences of the United States of America. **101**, 12130-12135
21 Paolini, L., Radeghieri, A., Civini, S., Caimi, L. and Ricotta, D. (2011) The Epsilon Hinge-Ear Region Regulates Membrane Localization of the AP-4 Complex. Traffic. **12**, 1604-1619
22 Alvisi, G., Musiani, D., Jans, D. A. and Ripalti, A. (2007) An importin alpha/beta-recognized bipartite nuclear localization signal mediates targeting of the human herpes simplex virus type 1 DNA polymerase catalytic subunit pUL30 to the nucleus. Biochemistry. **46**, 9155-9163
23 Avanzi, S., Leoni, V., Rotola, A., Alviano, F., Solimando, L., Lanzoni, G., Bonsi, L., Di Luca, D., Marchionni, C., Alvisi, G. and Ripalti, A. (2013) Susceptibility of Human Placenta Derived Mesenchymal Stromal/Stem Cells to Human Herpesviruses Infection. PLoS One. **8**, e71412
24 Ruggieri, A., Dazert, E., Metz, P., Hofmann, S., Bergeest, J. P., Mazur, J., Bankhead, P., Hiet, M. S., Kallis, S., Alvisi, G., Samuel, C. E., Lohmann, V., Kaderali, L., Rohr, K., Frese, M., Stoecklin, G. and Bartenschlager, R. (2012) Dynamic Oscillation of Translation and Stress Granule Formation Mark the Cellular Response to Virus Infection. Cell Host & Microbe. **12**, 71-85
25 Hussain, N. K., Jenna, S., Glogauer, M., Quinn, C. C., Wasiak, S., Guipponi, M., Antonarakis, S. E., Kay, B. K., Stossel, T. P., Lamarche-Vane, N. and McPherson, P. S. (2001) Endocytic protein intersectin-l regulates actin assembly via Cdc42 and N-WASP. Nature cell biology. **3**, 927-932
26 Alvisi, G., Marin, O., Pari, G., Mancini, M., Avanzi, S., Loregian, A., Jans, D. A. and Ripalti, A. (2011) Multiple phosphorylation sites at the C-terminus regulate nuclear import of HCMV DNA polymerase processivity factor ppUL44. Virology. **417**, 259-267
27 Scaturro, P., Trist, I. M., Paul, D., Kumar, A., Acosta, E. G., Byrd, C. M., Jordan, R., Brancale, A. and Bartenschlager, R. (2014) Characterization of the mode-of-action of a potent Dengue virus capsid inhibitor. J Virol
28 Alvisi, G., Jans, D., Guo, J., Pinna, L. and Ripalti, A. (2005) A protein kinase CK2 site flanking the nuclear targeting signal enhances nuclear transport of human cytomegalovirus ppUL44. Traffic. **6**, 1002-1013
29 Alvisi, G., Madan, V. and Bartenschlager, R. (2011) Hepatitis C virus and host cell lipids: an intimate connection. RNA Biol. **8**, 258-269
30 Ghildyal, R., Ho, A., Dias, M., Soegiyono, L., Bardin, P. G., Tran, K. C., Teng, M. N. and Jans, D. A. (2009) The respiratory syncytial virus matrix protein possesses a Crm1-mediated nuclear export mechanism. J Virol. **83**, 5353-5362
31 Sinigalia, E., Alvisi, G., Segre, C. V., Mercorelli, B., Muratore, G., Winkler, M., Hsiao, H. H., Urlaub, H., Ripalti, A., Chiocca, S., Palu, G. and Loregian, A. (2012) The Human Cytomegalovirus DNA Polymerase Processivity Factor UL44 Is Modified by SUMO in a DNA-Dependent Manner. Plos One. **7**, 18
32 Christie, M., Chang, C. W., Rona, G., Smith, K. M., Stewart, A. G., Takeda, A. A., Fontes, M. R., Stewart, M., Vertessy, B. G., Forwood, J. K. and Kobe, B. (2016) Structural Biology and Regulation of Protein Import into the Nucleus. J Mol Biol. **428**, 2060-2090

685 33 Alvisi, G., Avanzi, S., Musiani, D., Camozzi, D., Leoni, V., Ly-Huynh, J. D. and Ripalti, A. (2008) Nuclear
686 import of HSV-1 DNA polymerase processivity factor UL42 is mediated by a C-terminally located bipartite
687 nuclear localization signal. Biochemistry. **47**, 13764-13777
688 34 Di Noto, G., Chiarini, M., Paolini, L., Mazzoldi, E., Giustini, V., Radeghieri, A., Caimi, L. and Ricotta, D.
689 (2014) Immunoglobulin free light chains and GAGs mediate multiple myeloma extracellular vesicles uptake
690 and secondary NfkB nuclear translocation. Frontiers in immunology. **5**, 517
691 35 Lecat, S., Matthes, H. W., Pepperkok, R., Simpson, J. C. and Galzi, J. L. (2015) A Fluorescent Live
692 Imaging Screening Assay Based on Translocation Criteria Identifies Novel Cytoplasmic Proteins Implicated in
693 G Protein-coupled Receptor Signaling Pathways. Molecular & cellular proteomics : MCP. **14**, 1385-1399
694 36 Sinigalia, E., Alvisi, G., Mercorelli, B., Coen, D. M., Pari, G. S., Jans, D. A., Ripalti, A., Palu, G. and
695 Loregian, A. (2008) Role of homodimerization of human cytomegalovirus DNA polymerase accessory
696 protein UL44 in origin-dependent DNA replication in cells. J Virol. **82**, 12574-12579
697 37 Kuusisto, H. V., Wagstaff, K. M., Alvisi, G. and Jans, D. A. (2008) The C-terminus of apoptin
698 represents a unique tumor cell-enhanced nuclear targeting module. Int J Cancer. **123**, 2965-2969
699 38 Kosugi, S., Hasebe, M., Tomita, M. and Yanagawa, H. (2009) Systematic identification of cell cycle-
700 dependent yeast nucleocytoplasmic shuttling proteins by prediction of composite motifs. Proc Natl Acad Sci
701 USA. **106**, 10171-10176
702 39 Brar, S. S., Watson, M. and Diaz, M. (2004) Activation-induced cytosine deaminase (AID) is actively
703 exported out of the nucleus but retained by the induction of DNA breaks. J Biol Chem. **279**, 26395-26401
704 40 Radeghieri, A., Savio, G., Zendrini, A., Di Noto, G., Salvi, A., Bergese, P. and Piovani, G. (2017)
705 Cultured human amniocytes express hTERT, which is distributed between nucleus and cytoplasm and is
706 secreted in extracellular vesicles. Biochemical and biophysical research communications. **483**, 706-711
707 41 Alvisi, G., Roth, D. M., Camozzi, D., Pari, G. S., Loregian, A., Ripalti, A. and Jans, D. A. (2009) The
708 flexible loop of the human cytomegalovirus DNA polymerase processivity factor ppUL44 is required for
709 efficient DNA binding and replication in cells. J Virol. **83**, 9567-9576
710 42 Borroni, B., Archetti, S., Costanzi, C., Grassi, M., Ferrari, M., Radeghieri, A., Caimi, L., Caltagirone, C.,
711 Di Luca, M. and Padovani, A. (2009) Role of BDNF Val66Met functional polymorphism in Alzheimer's
712 disease-related depression. Neurobiology of aging. **30**, 1406-1412
713 43 Nabbi, A. and Riabowol, K. (2015) Rapid Isolation of Nuclei from Cells In Vitro. Cold Spring Harb
714 Protoc. **2015**, 769-772
715 44 Qiu, H. B. and Wang, Y. S. (2009) Exploring DNA-Binding Proteins with In Vivo Chemical Cross-
716 Linking and Mass Spectrometry. Journal of Proteome Research. **8**, 1983-1991
717 45 Henrich S, C. S., Crossett B, Baker MS, Christopherson RI. (2007) The nuclear proteome and DNA-
718 binding fraction of human Raji lymphoma cells. Biochimica et biophysica acta. **1774**
719 46 Henrich, S., Cordwell, S. J., Crossett, B., Baker, M. S. and Christopherson, R. I. (2007) The nuclear
720 proteome and DNA-binding fraction of human Raji lymphoma cells. Biochimica et biophysica acta. **1774**,
721 413-432
722 47 Paolini, L., Di Noto, G., Maffina, F., Martellosio, G., Radeghieri, A., Luigi, C. and Ricotta, D. (2015)
723 Comparison of Hevylite™ IgA and IgG assay with conventional techniques for the diagnosis and follow-up of
724 plasma cell dyscrasia. Annals of Clinical Biochemistry: An international journal of biochemistry and
725 laboratory medicine. **52**, 337-345
726 48 Paolini, L., Orizio, F., Busatto, S., Radeghieri, A., Bresciani, R., Bergese, P. and Monti, E. (2017)
727 Exosomes Secreted by HeLa Cells Shuttle on Their Surface the Plasma Membrane-Associated Sialidase
728 NEU3. Biochemistry. **56**
729 49 Banach-Orlowska, M., Pilecka, I., Torun, A., Pyrzynska, B. and Miaczynska, M. (2009) Functional
730 characterization of the interactions between endosomal adaptor protein APPL1 and the NuRD co-repressor
731 complex. The Biochemical journal. **423**, 389-400
732 50 Ricke, R. and Bielinsky, A. K. (2005) Easy detection of chromatin binding proteins by the histone
733 association assay. Biological Procedures Online. **7**, 60-69
734 51 Predescu, S., Bardita, C. and Predescu, D. (2015) New insights into the functions of intersectin-1s.
735 Commun Integr Biol. **8**, e1034400

52 Gryaznova, T., Kropyvko, S., Burdyniuk, M., Gubar, O., Kryklyva, V., Tsyba, L. and Rynditch, A. (2015) Intersectin adaptor proteins are associated with actin-regulating protein WIP in invadopodia. Cellular signalling. **27**, 1499-1508
53 Humphries, A. C., Donnelly, S. K. and Way, M. (2014) Cdc42 and the Rho GEF intersectin-1 collaborate with Nck to promote N-WASP-dependent actin polymerisation. Journal of cell science. **127**, 673-685
54 Sakaba, T., Kononenko, N. L., Bacetic, J., Pechstein, A., Schmoranzer, J., Yao, L., Barth, H., Shupliakov, O., Kobler, O., Aktories, K. and Haucke, V. (2013) Fast neurotransmitter release regulated by the endocytic scaffold intersectin. Proceedings of the National Academy of Sciences of the United States of America. **110**, 8266-8271
55 Yoshimura, S. H., Kumeta, M. and Takeyasu, K. (2014) Structural mechanism of nuclear transport mediated by importin beta and flexible amphiphilic proteins. Structure. **22**, 1699-1710
56 Vecchi, M., Polo, S., Poupon, V., van de Loo, J. W., Benmerah, A. and Di Fiore, P. P. (2001) Nucleocytoplasmic shuttling of endocytic proteins. The Journal of cell biology. **153**, 1511-1517
57 Poupon, V., Polo, S., Vecchi, M., Martin, G., Dautry-Varsat, A., Cerf-Bensussan, N., Di Fiore, P. P. and Benmerah, A. (2002) Differential nucleocytoplasmic trafficking between the related endocytic proteins Eps15 and Eps15R. The Journal of biological chemistry. **277**, 8941-8948
58 Mills, I. G., Gaughan, L., Robson, C., Ross, T., McCracken, S., Kelly, J. and Neal, D. E. (2005) Huntingtin interacting protein 1 modulates the transcriptional activity of nuclear hormone receptors. J Cell Biol. **170**, 191-200
59 Fontes, M. R., Teh, T. and Kobe, B. (2000) Structural basis of recognition of monopartite and bipartite nuclear localization sequences by mammalian importin-alpha. J Mol Biol. **297**, 1183-1194
60 Jeffery, C. J. (2014) An introduction to protein moonlighting. Biochemical Society transactions. **42**, 1679-1683
61 Honda, T. and Nakajima, K. (2006) Mouse Disabled1 (DAB1) is a nucleocytoplasmic shuttling protein. The Journal of biological chemistry. **281**, 38951-38965
62 Hyman, J., Chen, H., Di Fiore, P. P., De Camilli, P. and Brunger, A. T. (2000) Epsin 1 undergoes nucleocytosolic shuttling and its eps15 interactor NH(2)-terminal homology (ENTH) domain, structurally similar to Armadillo and HEAT repeats, interacts with the transcription factor promyelocytic leukemia Zn(2)+ finger protein (PLZF). The Journal of cell biology. **149**, 537-546
63 Dong, J. M., Lau, L. S., Ng, Y. W., Lim, L. and Manser, E. (2009) Paxillin nuclear-cytoplasmic localization is regulated by phosphorylation of the LD4 motif: evidence that nuclear paxillin promotes cell proliferation. The Biochemical journal. **418**, 173-184
64 Pekar, O., Benjamin, S., Weidberg, H., Smaldone, S., Ramirez, F. and Horowitz, M. (2012) EHD2 shuttles to the nucleus and represses transcription. The Biochemical journal. **444**, 383-394
65 Chaumet, A., Wright, G. D., Seet, S. H., Tham, K. M., Gounko, N. V. and Bard, F. (2015) Nuclear envelope-associated endosomes deliver surface proteins to the nucleus. Nat Commun. **6**, 8218
66 Yeh, C. T., Wong, S. W., Fung, Y. K. and Ou, J. H. (1993) Cell cycle regulation of nuclear localization of hepatitis B virus core protein. Proceedings of the National Academy of Sciences of the United States of America. **90**, 6459-6463
67 Yu, X. and Baer, R. (2000) Nuclear localization and cell cycle-specific expression of CtIP, a protein that associates with the BRCA1 tumor suppressor. The Journal of biological chemistry. **275**, 18541-18549
68 Alvisi, G. and Jans, D. A. (2015) Regulating post-mitotic nuclear access: Cdk1-phosphorylation of NLSs. Cell cycle. **14**, 695-696
69 Mosesson, Y., Mills, G. B. and Yarden, Y. (2008) Derailed endocytosis: an emerging feature of cancer. Nature reviews. Cancer. **8**, 835-850
70 Mellman, I. and Yarden, Y. (2013) Endocytosis and cancer. Cold Spring Harbor perspectives in biology. **5**, a016949
71 Song, J., Mu, Y., Li, C., Bergh, A., Miaczynska, M., Heldin, C. H. and Landstrom, M. (2016) APPL proteins promote TGFbeta-induced nuclear transport of the TGFbeta type I receptor intracellular domain. Oncotarget. **7**, 279-292

72 Gu, F., Zhang, H., Qin, F., Liu, X., Li, W., Fu, L., Ying, G., Li, B., Zhang, M. and Ma, Y. (2015) Intersectin1-S, a multidomain adapter protein, is essential for malignant glioma proliferation. Glia. **63**, 1595-1605

73 Russo, A. and O'Bryan, J. P. (2012) Intersectin 1 is required for neuroblastoma tumorigenesis. Oncogene. **31**, 4828-4834

FIGURE LEGENDS

Fig. 1 A fraction of endogenous and overexpressed ITSN1-s localizes within the cell nucleus. (A) HeLa cells, untransfected or transfected to express FLAG-ITSN1-s, were processed for nucleus (N)/cytosol (C) separation and the obtained fractions subjected to SDS-PAGE/WB using the indicated antibodies. The image is representative of three independent experiments. (B) HeLa cells transfected to express FLAG-ITSN1-s were fixed with PFA and processed for CLSM as described in the Experimental section. The DAPI channel, depicting cell nuclei is shown on the *left panel*, the FITC channel, relative to FLAG-ITSN1-s is shown on the *middle panel*, whereas a merged image of both channels is shown on the *right panel*. Scale bars, 5 μm. The inset represent a 1,5X magnification of the boxed area.

Fig. 2 Nuclear ITSN1-s is associated with the nuclear envelope. (A) 48 h after being transfected to express FLAG-ITSN1-s, HeLa cells were lysed and processed as described in the Experimental section to obtain whole cell lysate (W), cytosol (C), nuclei (N), nucleoplasm (NP) and nuclear envelope (NE) fractions. The respective distribution of the indicated proteins was investigated by SDS-PAGE/WB using the indicated antibodies, as described in the Experimental section. The amounts loaded were W 10%, C 30%, N 5%, NP 25%, NE 25% of the total cell extracts, respectively. The image is representative of three independent experiments. (B) FLAG-ITSN1-s transfected HeLa cells were fixed with 4% PFA, and processed for IF as described in the Experimental section to allow detection of FLAG-ITSN1-s (*left panel*), lamin A/C (*middle panel*), cell nuclei (DAPI, *right panel*). A merged image of all channels is shown on the right. Scale bars, 5 μm. The inset represents a 1,5 X magnification of the boxed area. Shown is a representative image chosen among three independent experiments. (C) HeLa cells were harvested, and 500 μg of the whole cell lysates were immunoprecipitated either in the presence of the α-ITSN1-s endogenous, α-lamin A/C or in the absence (k-) of antibodies, as described in the Experimental section. After SDS-PAGE/WB, purified proteins were detected using α-ITSN endogenous or α-lamin A/C antibodies. Whole cell lysates [50 μg (I)] were also loaded as further reference. The image is representative of three independent experiments.

(D) HeLa cells were treated with PFA 1% and processed to obtain a homogenate fraction (H, 50 µg) and DNA protein complexes (DPC, 10 cm dish content) as described in the Experimental section. Fractions were analyzed by SDS-PAGE/WB using the α-ITSN endogenous, α-tubulin and α-histone H3 (H3) antibodies. The image is representative of three independent experiments.

Fig. 3 ITSN1-s contains several putative NTSs. The primary sequences of ITSN1-s (NCBI Accession Number: NP_001001132.1) was scanned for putative NLS and NES using different bioinformatics tools, as described in the Experimental section. (A) A graphic representation of ITSN1s multi-domain structure is shown, along with the respective position of putative NLS (NLS; *gray oval*), and NESs (A-F; *blue stars*). Epsin-like domains (EH; *orange ovals*). Coiled coil domain (CC; *red square*). Src-Homology 3 domains (SH3; *green hexagons*). (B) The sequence of each putative NLS and NES is shown, along with the method used for their identification and a color code, indicating the position with respect to ITSN1-s domains identical to that used in panel a. The single letter amino acid code is used. Basic residues forming the putative NLS are in *bold face*. Hydrophobic residues forming putative NESs are *underlined.*

Fig. 4 ITSN1-s interacts with IMPα.(A) HEK 293-T cells were transfected to express GFP-IMPαΔIBB in the presence of FLAG-UL44. Cells were harvested 48 h after transfection and 500 µg of whole cell lysates were immunoprecipitated either in the presence (FLAG) or in the absence (k-) of the α-FLAG mAb, as described in the Experimental section. Whole cell lysates [50 µg (I)], and immunoprecipitated proteins (IP) were separated by SDS-PAGE/WB and the presence of the indicated proteins revealed using either α-FLAG or α-GFP mAbs. (B) HEK 293-T cells were transfected to express GFP-IMPαΔIBB in the presence of (+), or in the absence (-) of FLAG-ITSN1-s. Cells were harvested 48 h after transfection and 1 mg of transfected cell lysates was immunoprecipitated in the presence of the α-FLAG mAb, as described in the Experimental section. Whole cell lysates [50 µg (I)] and immunoprecipitated proteins (IP-FLAG) were separated by SDS-PAGE/WB, and purified proteins were detected using either α-FLAG or α-GFP mAbs The image is representative of three independent experiments.

Fig. 5 ITSN1-s shuttles between nucleus and cytoplasm in a CRM-1 dependent fashion. HeLa cells were transfected to transiently express FLAG-ITSN1-s. Eight hours before processing samples for IF and CLSM analysis, cells were treated either with LMB (2.9 ng/µl 0.01% Methanol) or with solvent (0.01% Methanol). (A) Representative microscopic images of cells treated with solvent (-LMB; *top panels*), or LMB (+ LMB; *bottom panels*) are shown relative to ITSN1s (*first panels*),

lamin A/C (*second panels*) and nuclei (*DAPI, third panels*). A merged image is shown (*right panels*). Scale bars, 5 μm. (B) Digital images such as those shown in (A) were quantitatively analyzed using software ImageJ to calculate the Fn/c ratio relative to ITSN1-s, as described in the Experimental section. The mean ± SEM relative to at least three independent experiments (n ≥3) is shown, along with the *p* value relative to the Student *t*-test between LMB treated and untreated cells. ** = $p \leq 0.01$

Fig. 6 ITSN1-s CC and SH3 regions can independently undergo nucleocytoplasmic shuttling. (A) HEK 293 cells were transfected to transiently express the indicated YFP-ITSN1-s fusion proteins. The presence of the putative NLS (NLS; *gray oval*), and NESs (A-F; *blue stars*) is indicated. (B) 48 h post transfections cells were lysed and processed as described in the Experimental section for SDS-PAGE/WB analysis, to allow detection of the indicated fusion protein using a polyclonal α-GFP antibody. The presence of the YFP-ITSN1-s fusion of interest at the expected molecular weight is indicated by a pink arrowhead, whereas the presence of YFP-ITSN-CC aggregates of higher molecular weight is highlighted by black arrowheads. The image is representative of three independent experiments. (C) Eight hours before being processed for imaging by CLSM, cells were treated with either LMB (2.9 ng/μl 0.01% Methanol) or solvent (0.01% Methanol). Representative microscopic images of cells treated with solvent (- LMB; *top panels*), or LMB (+ LMB; *bottom panels*) are shown. Scale bars, 10 μm (D) Digital images such as shown in (C) were quantitatively analyzed using software ImageJ to calculate the Fn/c ratio relative to the indicated proteins, as described in the Experimental section. The mean ± SEM relative to at least three independent experiments is shown, along with the *p* value relative to the Student *t* test between LMB treated and untreated cells. * = $p \leq 0.05$

Fig. 7 ITSN1-s residues 1104-1127 represent a bipartite cNLS able to confer energy dependent nuclear targeting properties to heterologous proteins. (A) HEK 293-A cells were transfected to transiently express the indicated fusion proteins. Thirty min before processing the cells for CLSM analysis, media was changed either with fresh DMEM (+ ATP, *left panels*) or with an energy depletion media (- ATP, *right panels*; see Experimental section). Scale bars, 10 μm (B) Digital images such as those shown in (A) were quantitatively analyzed using software ImageJ to calculate the Fn/c ratio relative to each fusion protein, as described in the Experimental section. The mean ± SEM relative to pooled data from two independent experiments (n > 40) is shown, along with the *p* value relative to the Student *t* test between cells expressing YFP-NLS fusions and

YFP alone in the presence of ATP, or relative to cells expressing the individual YFP fusions, in the presence or in the absence of ATP . * = $p \leq 0.05$

Fig. 8 ISTN-NLS is important for ITSN-SH3 region nuclear accumulation. (A) HEK 293-A cells were transfected to transiently express the YFP-ITSN1s fusions shown. The presence of the putative NLS (NLS; *gray oval*), and NESs (A-F; *blue stars*) is indicated. Mutated NLS are shown as *black ovals*. (B) Six hours before being processed for CLSM analysis, cells were treated with either LMB (2.9 ng/µl in 0.01% Methanol) or solvent (0.01% Methanol). Representative images relative to the indicated YFP-ITSN1s point mutant are shown either in the absence (- LMB, *upper panels*) or in the presence (+ LMB, *bottom panels*) of LMB. Scale bars, 10 µm (C) Digital images such as those shown in (B) were quantitatively analyzed using software ImageJ to calculate the Fn/c ratio relative to each fusion protein, as described in the Experimental section. The mean ± SEM relative to at least three independent experiments is shown, along with the *p* value relative to the Student *t* test between the indicated conditions. * = $p \leq 0.05$

Fig. 9 ITSN1s-CC possesses an intrinsic capability to undergo nucleocytoplasmic shuttling. (A) HEK 293-A cells were transfected to transiently express the YFP-ITSN1-s fusions shown. The presence of the putative NLS (NLS; *gray oval*), and NESs (A-F; *blue stars*) is indicated. Mutated NLS are shown as *black ovals*. (B) Six hours before being processed for CLSM analysis, cells were treated with either LMB (2.9 ng/µl 0.01% Methanol) or solvent (0.01% Methanol). Representative images relative to the indicated YFP-ITSN1s point mutant are shown either in the absence (- LMB; *upper panels*) or in the presence (+ LMB; *bottom panels*) of LMB. Scale bars, 10 µm (C) Digital images such as those shown in (B) were quantitatively analyzed using software ImageJ to calculate the Fn/c ratio relative to each fusion protein, as described in the Experimental section. The mean ± SEM is shown ($n \geq 3$), along with the *p* value relative to the Student *t* test between LMB treated and untreated cells. * = $p \leq 0.05$

Fig. S1 GFP-fusion proteins were used as controls for LMB treatment. (A) HeLa cells were transfected to transiently express GFP, GFP-REV or GFP-UL44. Eight hours before processing samples for IF and CLSM analysis, cells were treated either with LMB (2.9 ng/µl 0.01% Methanol) or with solvent (0.01% Methanol). Representative microscopic images of cells treated with solvent (- LMB; *top panels*), or LMB (+ LMB; *bottom panels*) are shown relative to different constructs. A

merged image, including DAPI staining to facilitate visualization of cell nuclei is shown (*right panels*). (B) Digital images such as shown in (A) were quantitatively analyzed using software ImageJ to calculate the Fn/c ratio relative to GFP and GFP-fusions, as described in the Experimental section. The mean ± SEM relative to at least three independent experiments ($n \geq 3$) is shown. The *p* value relative to the Student *t*-test between LMB treated and untreated cells is shown. *** = $p \leq 0.001$

Fig S2. YFP-ITSN1-s allows direct visualization of ITSN1-s in living cells. HeLa cells were transfected to transiently express YFP-ITSN1-s and imaged live for 30 min using a Leica DMi8 inverted epifluorescent microscope. Images relative to Bright field and nuclei (not shown) as well as of the YFP channel (gray) were acquired every minute. Scale bars, 20 mM. Positions of a large (red arrow) and small (green arrow) ITSN1-s vesicles is shown.

Fig. S3. Time dependent nuclear accumulation of YFP-ITSN1-s in the nucleus of living cells upon addition of LMB. HeLa cells were transfected to transiently express YFP-ITSN1-s. 15 min after addition of LMB or vehicle, the subcellular localization of spontaneously fluorescent fusion proteins was monitored for 10h with a frequency of 15 min using a Leica DMi8 inverted epifluorescent microscope. (A) The subcellular localization of a cell expressing YFP-ITSN1-s is shown, along with the time after addition of LMB. (B) Quantification of the levels of nuclear accumulation of YFP-ITSN1-s at the indicated time points after the addition of LMB (*red circles*) or vehicle (*blue circles*). Data are the mean + standard error of the mean relative to > 5 cells. (C) Quantification of the levels of nuclear accumulation YFP-ITSN1-s (red circles) of the control fusion protein GFP-UL44DNLS (*blue circles*) at the indicated time points after addition of LMB. Data are the mean ± SEM relative to > 5 cells.

Movie S1. YFP-ITSN1-s allows direct visualization of ITSN1-s in living cells. HeLa cells were transfected to transiently express YFP-ITSN1-s and imaged live for 30 min using a Leica DMi8 inverted microscope. Images relative to Bright field and nuclei (not shown) as well as of the YFP channel (gray) were acquired every minute. Scale bars, 20 mM. Positions of a large (red arrow) and small (green arrow) ITSN1-s vesicles is shown.

Movie S2. Time dependent nuclear accumulation of YFP-ITSN1-s in the nucleus of living cells upon addition of LMB. HeLa cells were transfected to transiently express YFP-ITSN1-s. 15 min after addition of LMB or vehicle, the subcellular localization of spontaneously fluorescent fusion

proteins was monitored for 10h with a frequency of 15 min using a Leica DMi8 inverted epifluorescent microscope. The subcellular localization (top panels) and relative Fn/c quantification (*bottom panels*) relative to cells expressing YFP-ITSN1-s either in the absence (*left panels*) or presence (*midldle panels*) of LMB, as well as to cells expressing GFP-UL44DNLS after addition of LMB (*right panels*) is shown. Data are the mean ± SEM relative to > 5 cells.

Figure 1

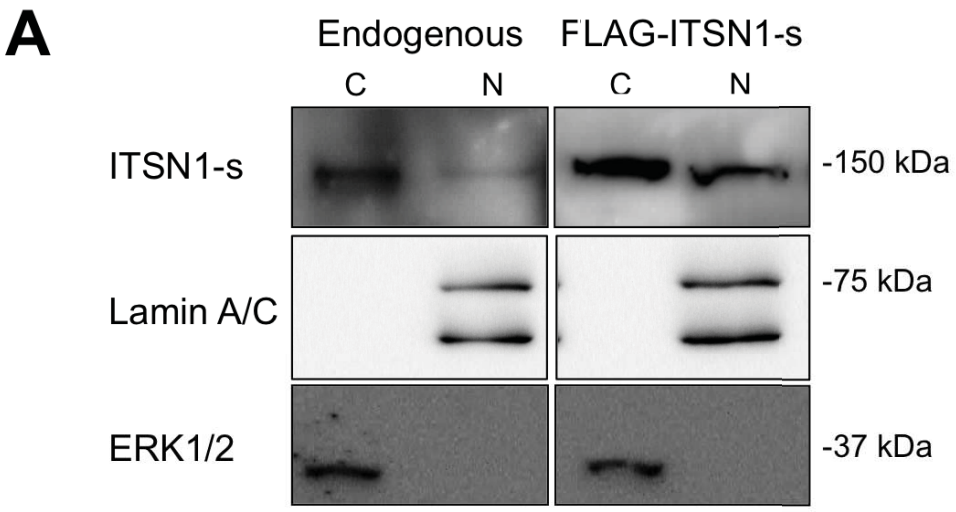
A
Endogenous
FLAG-ITSN1-s
C
N
C
N
ITSN1-s
Lamin A/C
ERK1/2
-150 kDa
-75 kDa
-37 kDa

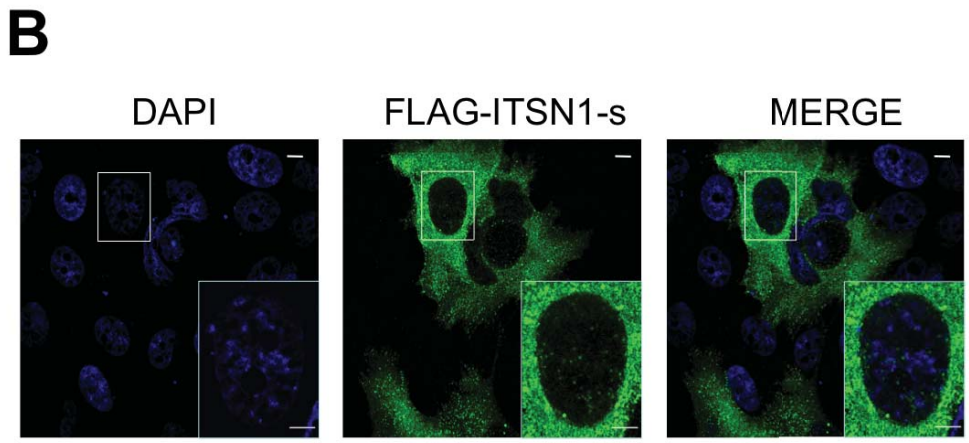
B
DAPI
FLAG-ITSN1-s
MERGE

Figure 2

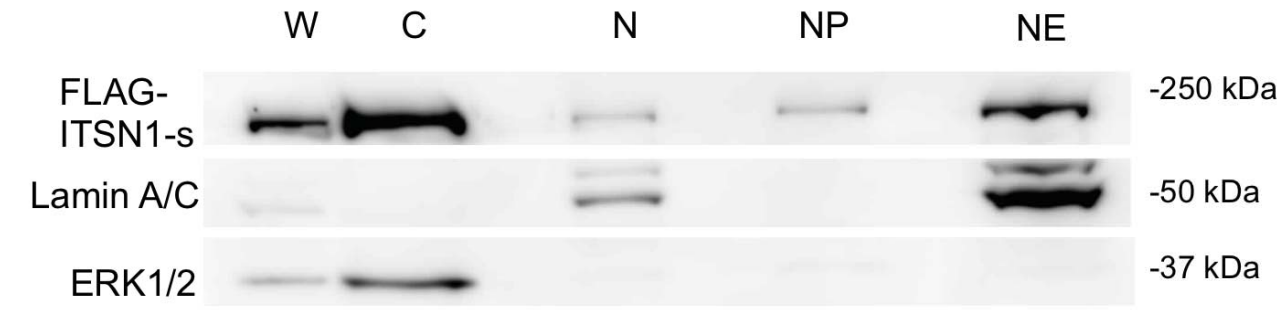
A
W
C
N
NP
NE
FLAG-ITSN1-s
Lamin A/C
ERK1/2
-250 kDa
-50 kDa
-37 kDa

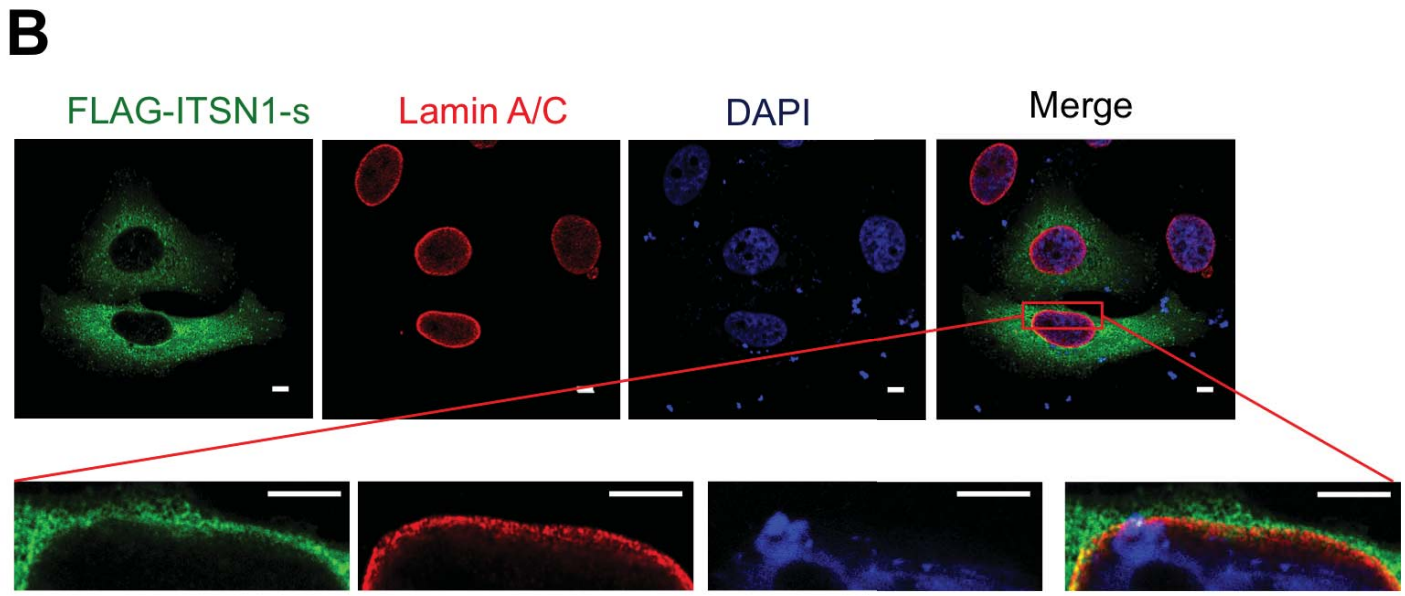
B
FLAG-ITSN1-s
Lamin A/C
DAPI
Merge

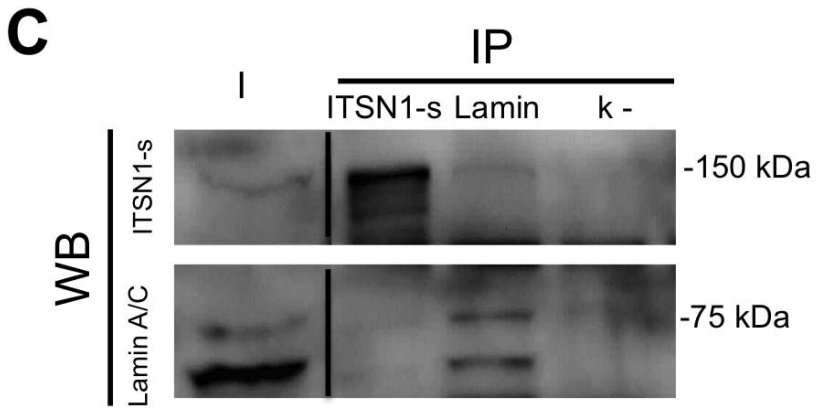
C
IP
I
ITSN1-s
Lamin
k -
WB
ITSN1-s
Lamin A/C
-150 kDa
-75 kDa

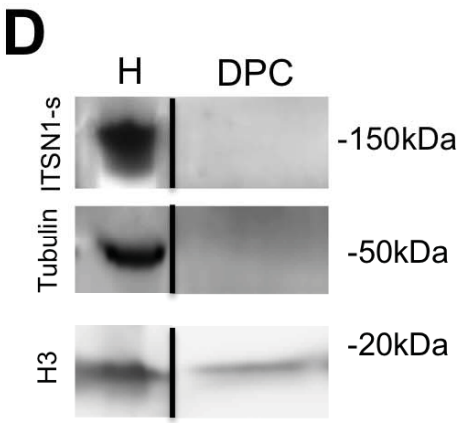
D
H
DPC
ITSN1-s
Tubulin
H3
-150kDa
-50kDa
-20kDa

Figure 3

A

B

SIGNAL NAME	SEQUENCE	METHOD
NESA	MDQVEFSIAMKLIKLKL 89	NES FINDER
NESB	ILMQSSLPQAQLASIWNL 265	VISUAL
NESC	FILAMHLIDVAM 290	NES FINDER
NESD	LELEKQLEKQREL 419	VISUAL
NESE	LTLAPGQLILI 1103	VISUAL
NESF	LAAVCQVIGM 1163	NES FINDER
NLS	**RKK**NPGGWWEGELQA**R**G**KKR**QIGW 1127	cNLS MAPPER

Figure 4

A

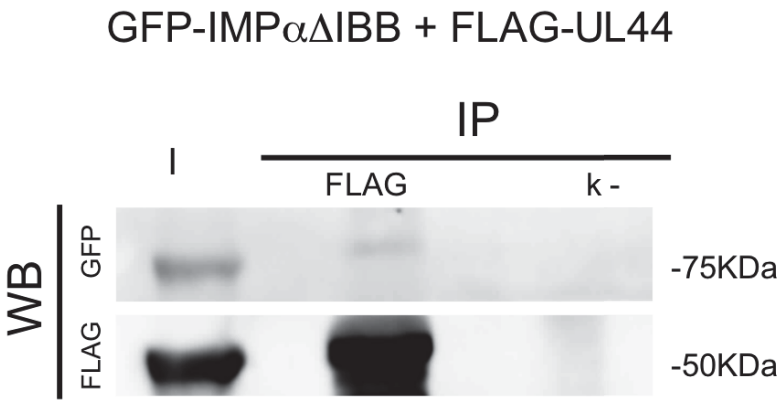
GFP-IMPαΔIBB + FLAG-UL44
IP
I
FLAG
k -
WB
GFP
FLAG
-75KDa
-50KDa

B

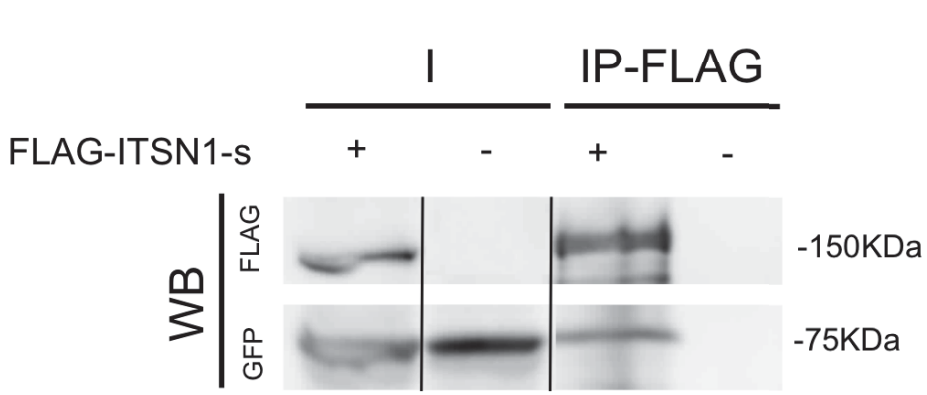
GFP-IMPαΔIBB ± FLAG-ITSN1-s
I
IP-FLAG
FLAG-ITSN1-s
+
-
+
-
WB
FLAG
GFP
-150KDa
-75KDa

Figure 5

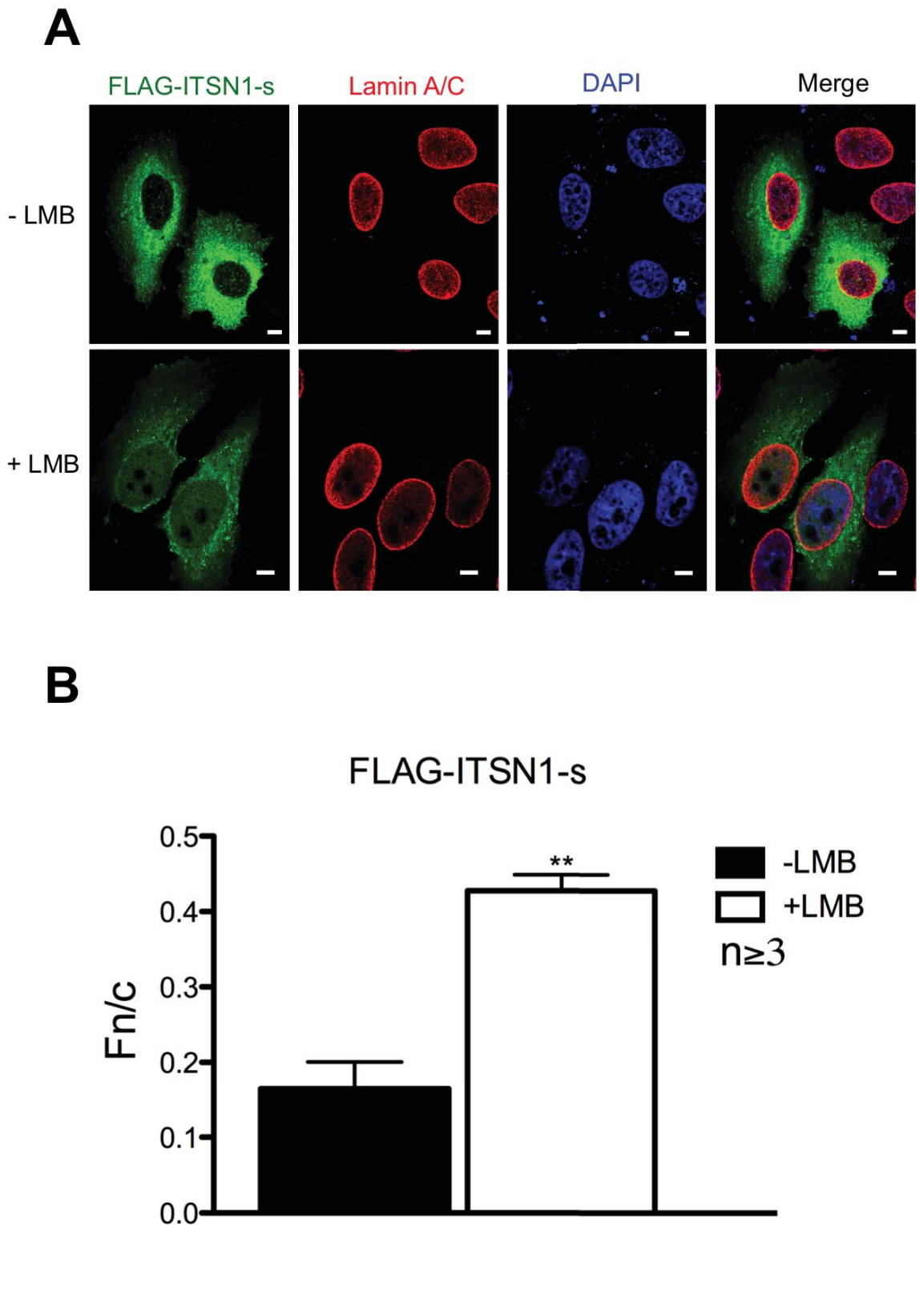
A
FLAG-ITSN1-s
Lamin A/C
DAPI
Merge
- LMB
+ LMB
B
FLAG-ITSN1-s
Fn/c
0.5
0.4
0.3
0.2
0.1
0.0
**
-LMB
+LMB
n≥3

Figure 6

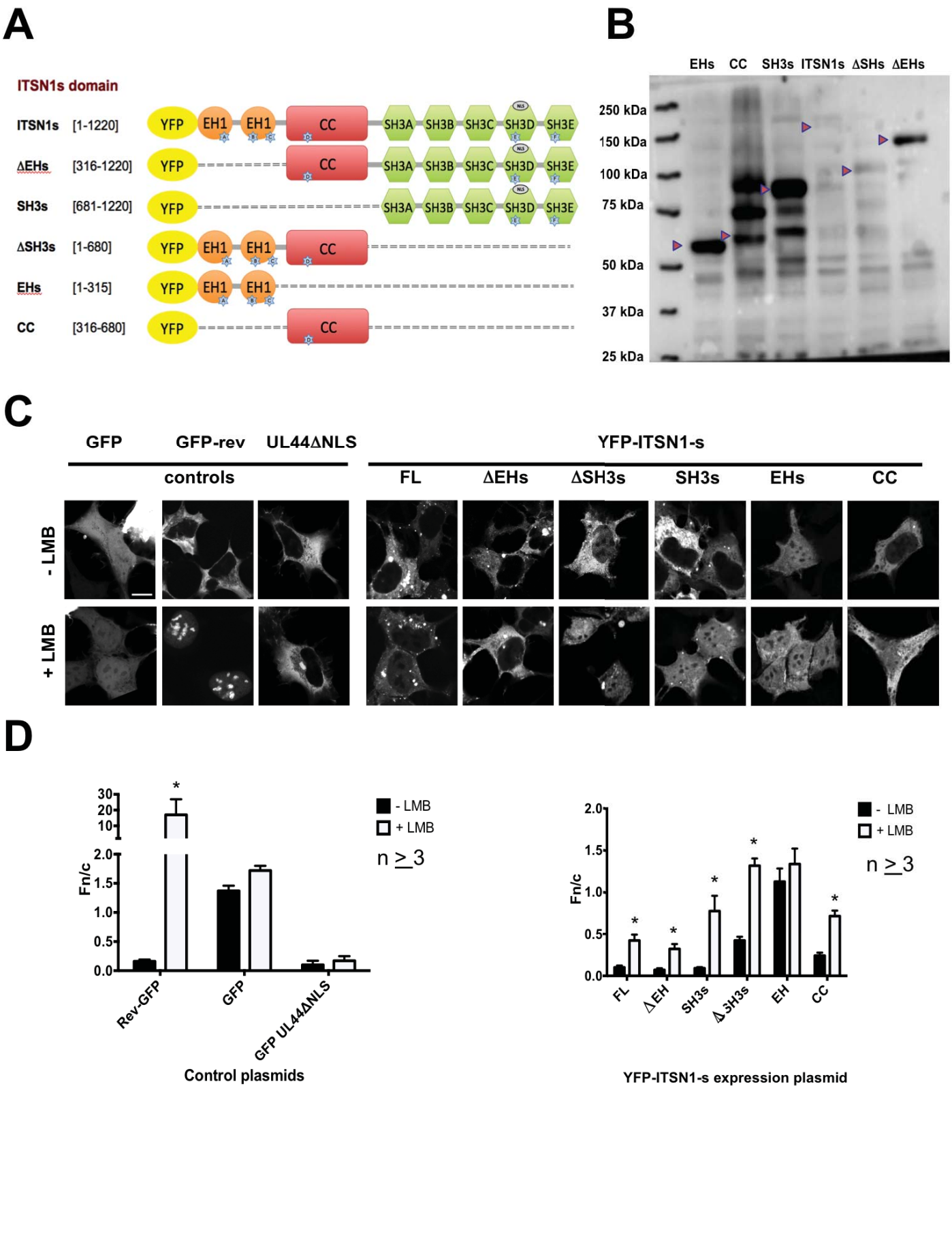
A
ITSN1s domain
ITSN1s [1-1220]
ΔEHs [316-1220]
SH3s [681-1220]
ΔSH3s [1-680]
EHs [1-315]
CC [316-680]
YFP
EH1
CC
SH3A
SH3B
SH3C
SH3D
SH3E
B
EHs
CC
SH3s
ITSN1s
ΔSHs
ΔEHs
250 kDa
150 kDa
100 kDa
75 kDa
50 kDa
37 kDa
25 kDa
C
GFP
GFP-rev
UL44ΔNLS
controls
YFP-ITSN1-s
FL
ΔEHs
ΔSH3s
SH3s
EHs
CC
- LMB
+ LMB
D
Fn/c
- LMB
+ LMB
n ≥ 3
Rev-GFP
GFP
GFP UL44ΔNLS
Control plasmids
FL
ΔEH
SH3s
ΔSH3s
EH
CC
YFP-ITSN1-s expression plasmid

Figure 7

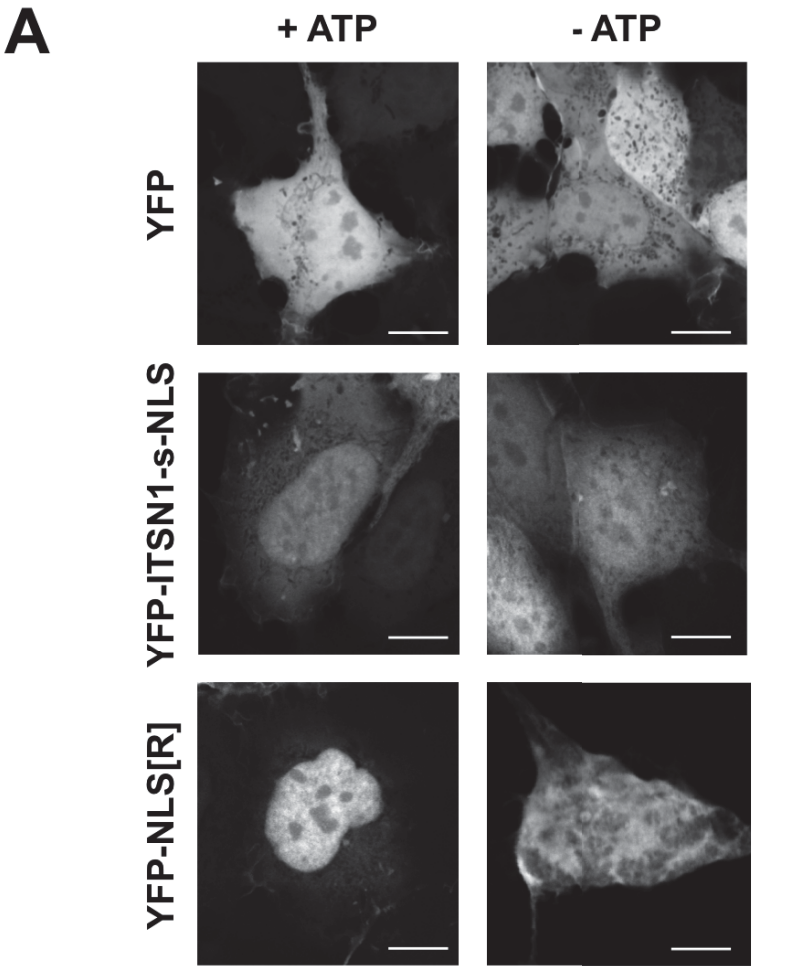
A
+ ATP
- ATP
YFP
YFP-ITSN1-s-NLS
YFP-NLS[R]
B
+ ATP
- ATP
n ≥ 40
Fn/c
0
1
2
3
YFP
YFP-ITSN1-s NLS
YFP-NLS[R]
Expression plasmid

Figure 8

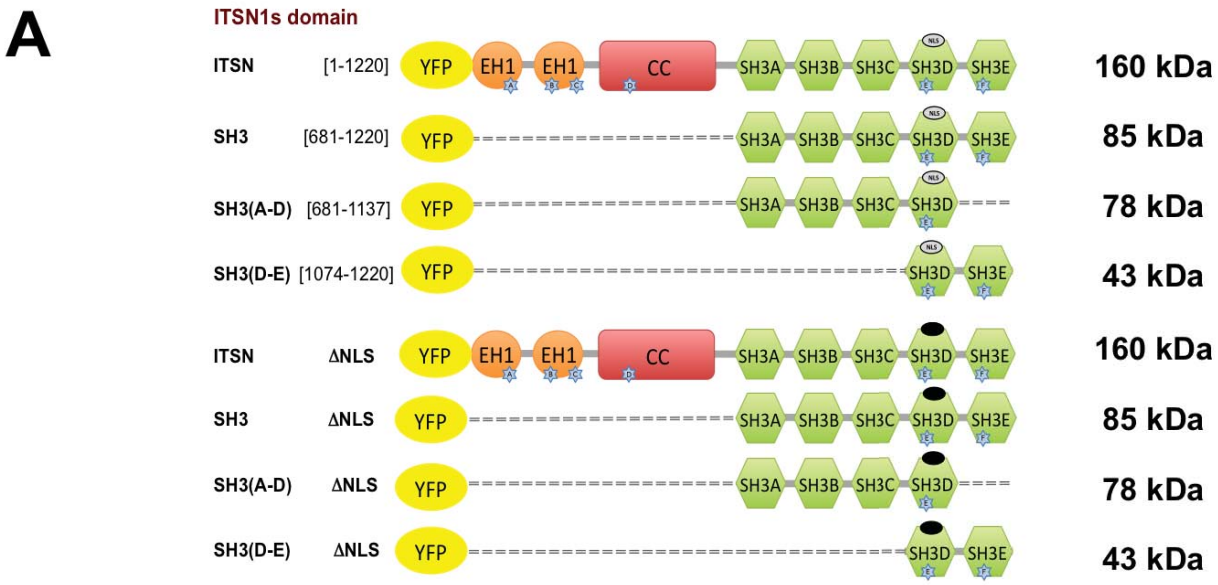
A
ITSN1s domain
ITSN [1-1220]
SH3 [681-1220]
SH3(A-D) [681-1137]
SH3(D-E) [1074-1220]
ITSN ΔNLS
SH3 ΔNLS
SH3(A-D) ΔNLS
SH3(D-E) ΔNLS
YFP
EH1
EH1
CC
SH3A
SH3B
SH3C
SH3D
SH3E
NLS
160 kDa
85 kDa
78 kDa
43 kDa
160 kDa
85 kDa
78 kDa
43 kDa

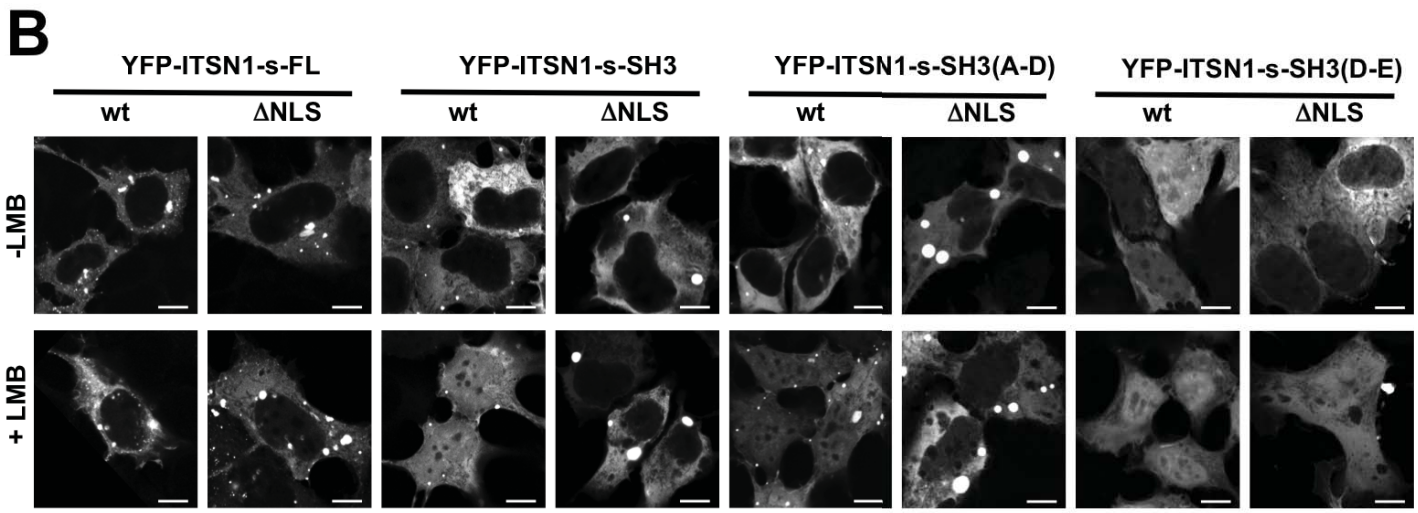
B
YFP-ITSN1-s-FL
YFP-ITSN1-s-SH3
YFP-ITSN1-s-SH3(A-D)
YFP-ITSN1-s-SH3(D-E)
wt
ΔNLS
wt
ΔNLS
wt
ΔNLS
wt
ΔNLS
-LMB
+ LMB

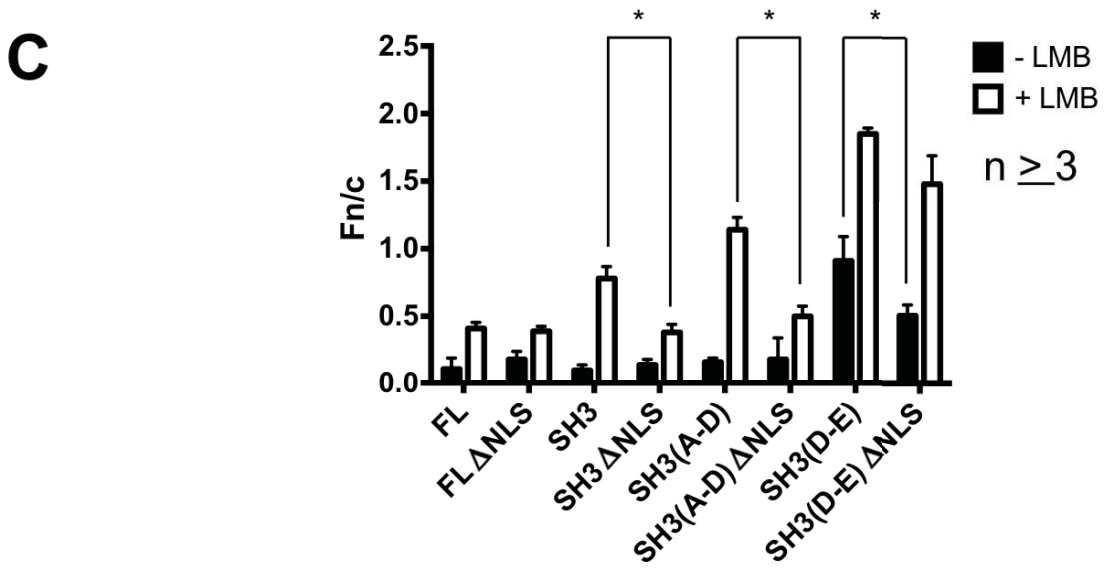
C
Fn/c
2.5
2.0
1.5
1.0
0.5
0.0
*
*
*
- LMB
+ LMB
n ≥ 3
FL
FL ΔNLS
SH3
SH3 ΔNLS
SH3(A-D)
SH3(A-D) ΔNLS
SH3(D-E)
SH3(D-E) ΔNLS
YFP-ITSN1-s expression plasmid

Figure 9

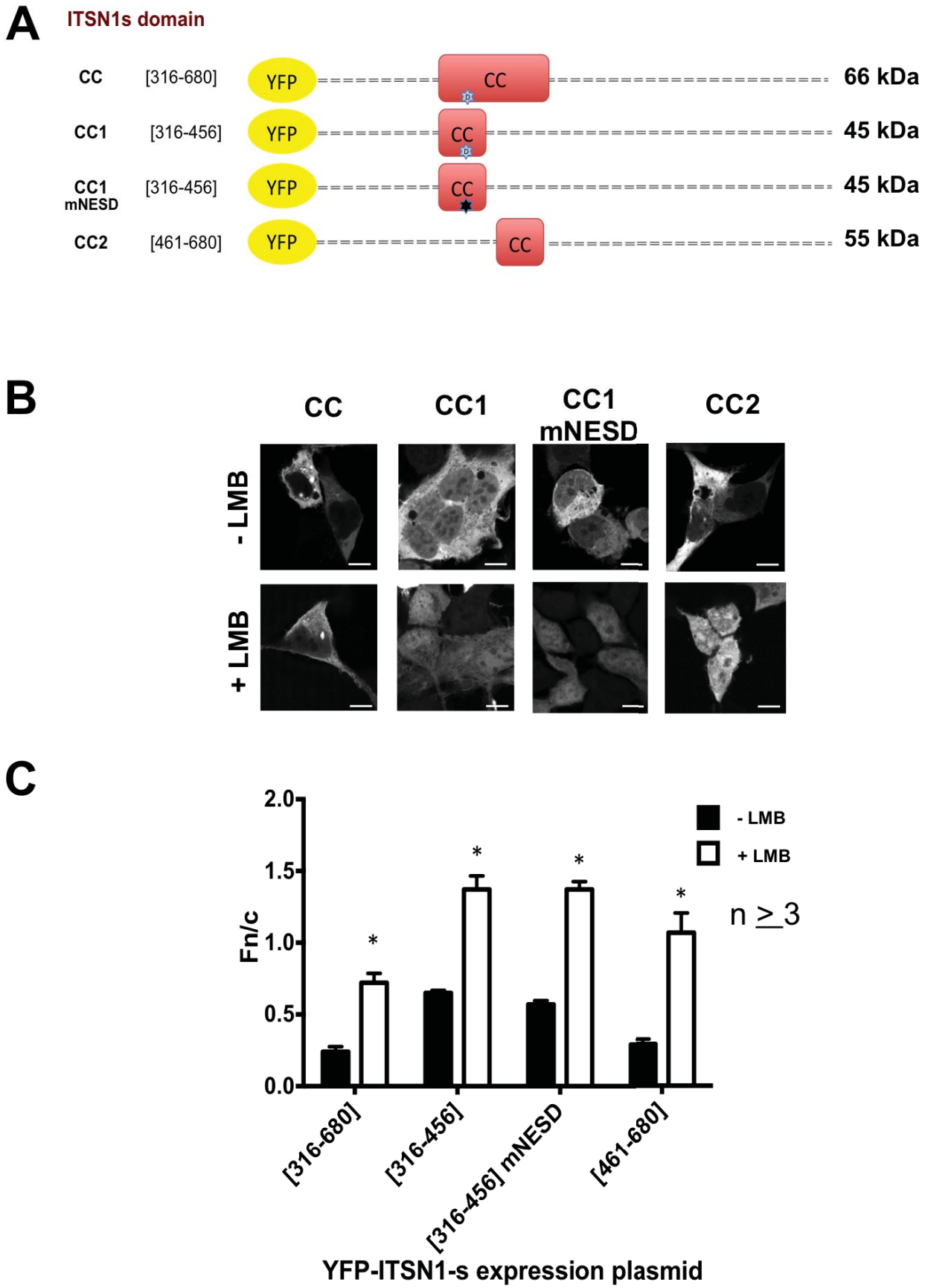
A
ITSN1s domain
CC [316-680] YFP CC 66 kDa
CC1 [316-456] YFP CC 45 kDa
CC1 mNESD [316-456] YFP CC 45 kDa
CC2 [461-680] YFP CC 55 kDa
B
CC
CC1
CC1 mNESD
CC2
- LMB
+ LMB
C
Fn/c
2.0
1.5
1.0
0.5
0.0
- LMB
+ LMB
n ≥ 3
[316-680]
[316-456]
[316-456] mNESD
[461-680]
YFP-ITSN1-s expression plasmid

Supplementary Table S1, data to Figure S1

	- LMB			+ LMB		
Plasmid	mean	S.E.M.	n	mean	S.E.M.	n
Rev-GFP	0.43	0.1	3	15.47	7.22	3
GFP UL44ΔNLS	0.24	0.13	4	0.3	0.07	4
GFP	1.23	0.1	3	1.53	0.3	3

Supplementary Table S1. Data to Figure S1. Digital images such as shown in Figure S1, were quantitatively analysed using software ImageJ to calculate the Fn/C ratio relative to the indicated proteins, as described in Material and Method section. For each experiment, an average of 30 cells was analyzed. The mean, and standard error of the mean (S.E.M.) relative to n experiments are shown.

Supplementary Table S2, data to Figure 5

	- LMB			+ LMB		
Plasmid	mean	S.E.M.	n	mean	S.E.M.	n
FLAG-ITSN1-s	0.17	0.02	3	0.43	0.02	3

Supplementary Table S2. Data to Figure 5. Digital images such as shown in Figure 5 were quantitatively analysed using software ImageJ to calculate the Fn/C ratio relative to the indicated proteins, as described in Material and Method section. For each experiment, an average of 30 cells was analyzed. The mean, and standard error of the mean (S.E.M.) relative to n experiments are shown.

Supplementary Table S3, data to Figure 6d, *left panels*

	- LMB			+ LMB		
Plasmid	mean	S.E.M.	n	mean	S.E.M.	n
Rev-GFP	0.16	0.06	8	19.31	4.00	7
GFP/YFP	1.27	0.05	7	1.50	0.11	6
GFP UL44ΔNLS	0.10	0.04	4	0.17	0.05	3

Supplementary Table S3. Data to Figure 6d, *left panels*. Digital images such as shown in Figure 6c, *left panel*, were quantitatively analysed using software ImageJ to calculate the Fn/C ratio relative to the indicated proteins, as described in Material and Method section. For each experiment, an average of 30 cells was analyzed. The mean, and standard error of the mean (S.E.M.) relative to n experiments are shown.

Supplementary Table S4, data to Figure 6d, *right panels*

	- LMB			+ LMB		
YFP-ITSN1-s	mean	S.E.M.	n	mean	S.E.M.	n
[1-1220]	0.11	0.03	7	0.41	0.04	6
[316-1220]	0.07	0.02	4	0.32	0.06	3
[1-680]	0.42	0.05	4	1.32	0.09	3
[1-315]	1.13	0.16	5	1.34	0.18	3
[316-680]	0.24	0.04	5	0.72	0.07	4
[681-1220]	0.10	0.01	9	0.78	0.09	8

Supplementary Table S4. Data to Figure 6d, *right panels*. Digital images such as shown in Figure 6c, *right panel*, were quantitatively analysed using software ImageJ to calculate the Fn/C ratio relative to the indicated proteins, as described in Material and Method section. For each experiment, an average of 30 cells was analyzed. The mean, and standard error of the mean (S.E.M.) relative to n experiments are shown.

Supplementary Table S5, data to Figure 7b

	YFP		YFP-ITSN-1s-NLS		YFP-NLS[R]	
	+ ATP	- ATP	+ ATP	- ATP	+ ATP	- ATP
Number of cells	215	105	104	52	83	43
Mean	1.110	1.179	1.830	1.351	2.810	1.469
S.E.M.	0.02	0.03	0.07	0.05	0.18	0.09

Supplementary Table S5. Data to Figure 7b. Digital images such as shown in Figure 7a, were quantitatively analysed using software ImageJ to calculate the Fn/C ratio relative to the indicated proteins, as described in Material and Method section. Data from two independent experiments were pooled. The mean and standard error of the mean (S.E.M.) relative the indicated number of cells are shown.

Supplementary Table S6, data to Figure 8c

	- LMB			+ LMB		
YFP-ITSN1-s	mean	S.E.M.	n	mean	S.E.M.	n
[1-1220]	0.11	0.03	7	0.41	0.04	6
[1-1220]-ΔNLS	0.18	0.03	3	0.39	0.03	3
[681-1220]	0.10	0.01	9	0.78	0.09	8
[681-1220]-Δ NLS	0.14	0.02	4	0.38	0.06	4
[681-1137]	0.16	0.02	3	1.14	0.09	3
[681-1137]-Δ NLS	0.18	0.09	3	0.50	0.08	3
[1074-1220]	0.91	0.06	9	1.85	0.04	8
[1074-1220]-Δ NLS	0.50	0.04	4	1.48	0.21	4

Supplementary Table S6. Data to Figure 8c. Digital images such as shown in Figure 8b, were quantitatively analysed using software ImageJ to calculate the Fn/C ratio relative to the indicated proteins, as described in Material and Method section. For each experiment, an average of 30 cells was analyzed. The mean, and standard error of the mean (S.E.M.) relative to n experiments are shown.

Supplementary Table S7, data to Figure 9c

		- LMB			+ LMB	
YFP-ITSN1-s	mean	S.E.M	n	mean	S.E.M.	n
[316-680]	0.24	0.04	5	0.72	0.07	4
[316-456]	0.65	0.02	5	1.37	0.10	4
[316-456]-mNESD	0.57	0.03	5	1.37	0.06	4
[461-680]	0.29	0.04	4	1.07	0.14	3

Supplementary Table S7. Data to Figure 9c. Digital images such as shown in Figure 9b, were quantitatively analysed using software ImageJ to calculate the Fn/C ratio relative to the indicated proteins, as described in Material and Method section. For each experiment, an average of 30 cells was analyzed. The mean, and standard error of the mean (S.E.M.) relative to n experiments are shown.

Figure S1

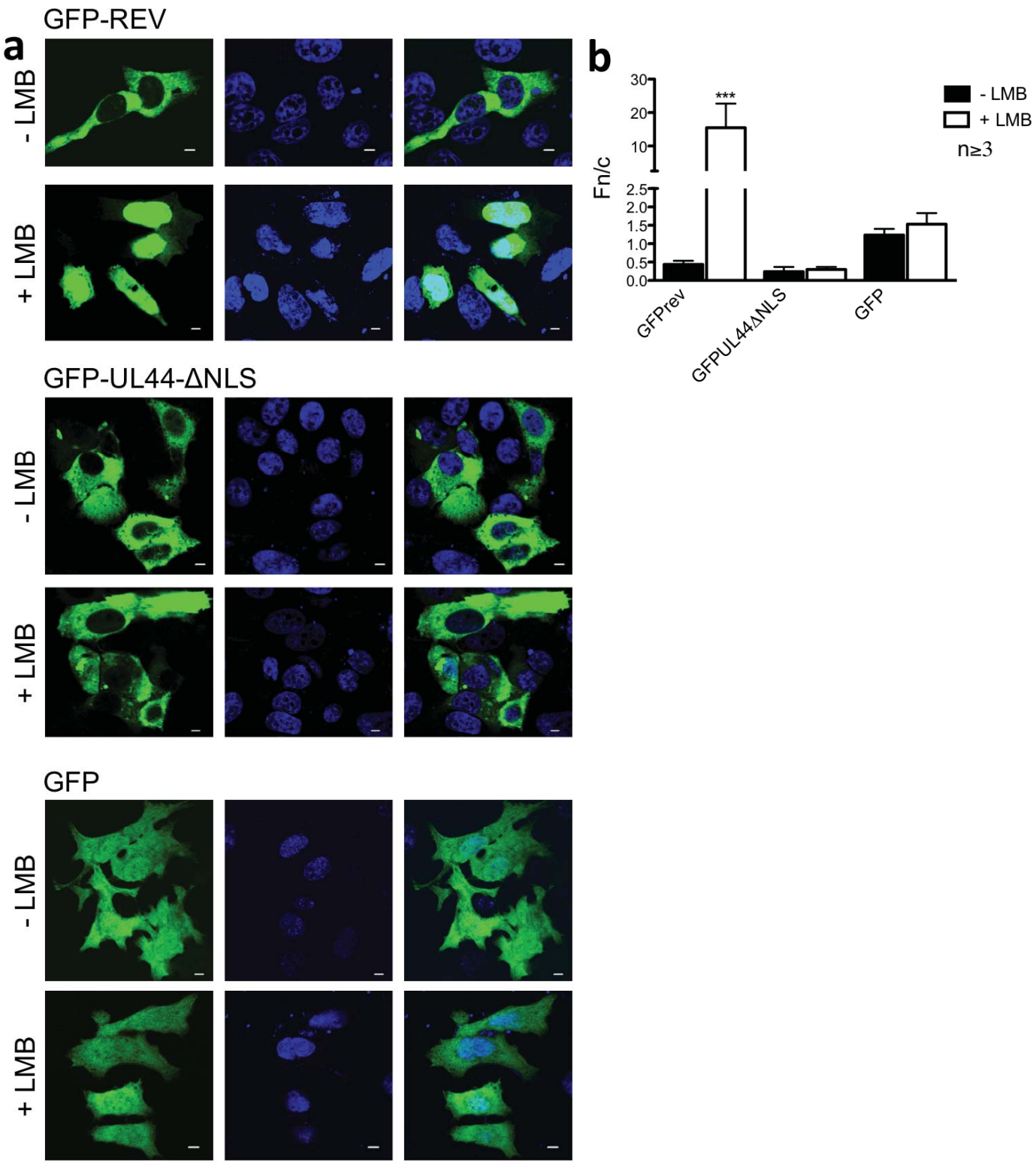
a
GFP-REV
- LMB
+ LMB
GFP-UL44-ΔNLS
- LMB
+ LMB
GFP
- LMB
+ LMB
b
Fn/c
30
20
10
2.5
2.0
1.5
1.0
0.5
0.0
***
- LMB
+ LMB
n≥3
GFPrev
GFPUL44ΔNLS
GFP

Figure S2

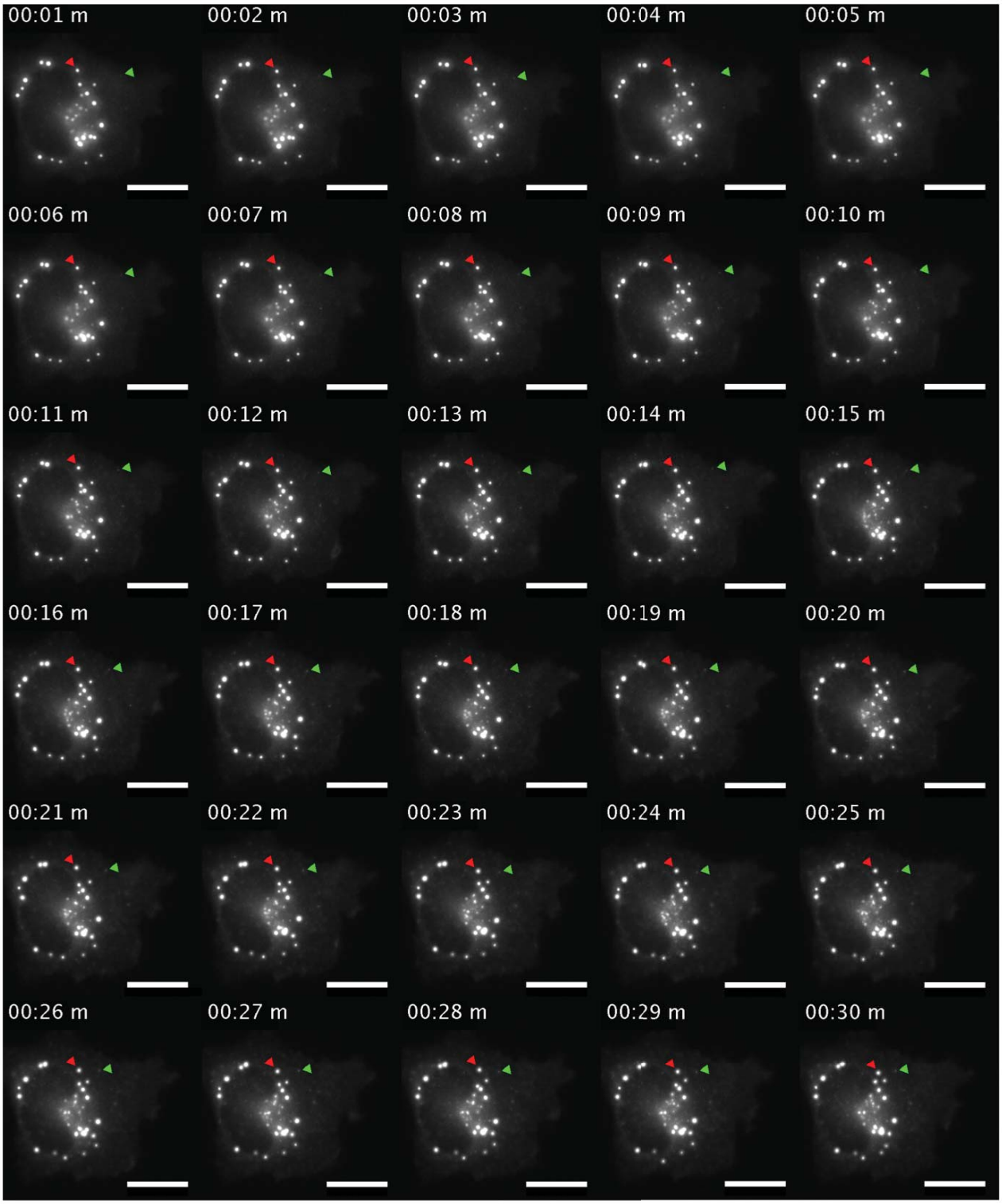
00:01 m
00:02 m
00:03 m
00:04 m
00:05 m
00:06 m
00:07 m
00:08 m
00:09 m
00:10 m
00:11 m
00:12 m
00:13 m
00:14 m
00:15 m
00:16 m
00:17 m
00:18 m
00:19 m
00:20 m
00:21 m
00:22 m
00:23 m
00:24 m
00:25 m
00:26 m
00:27 m
00:28 m
00:29 m
00:30 m

Figure S3

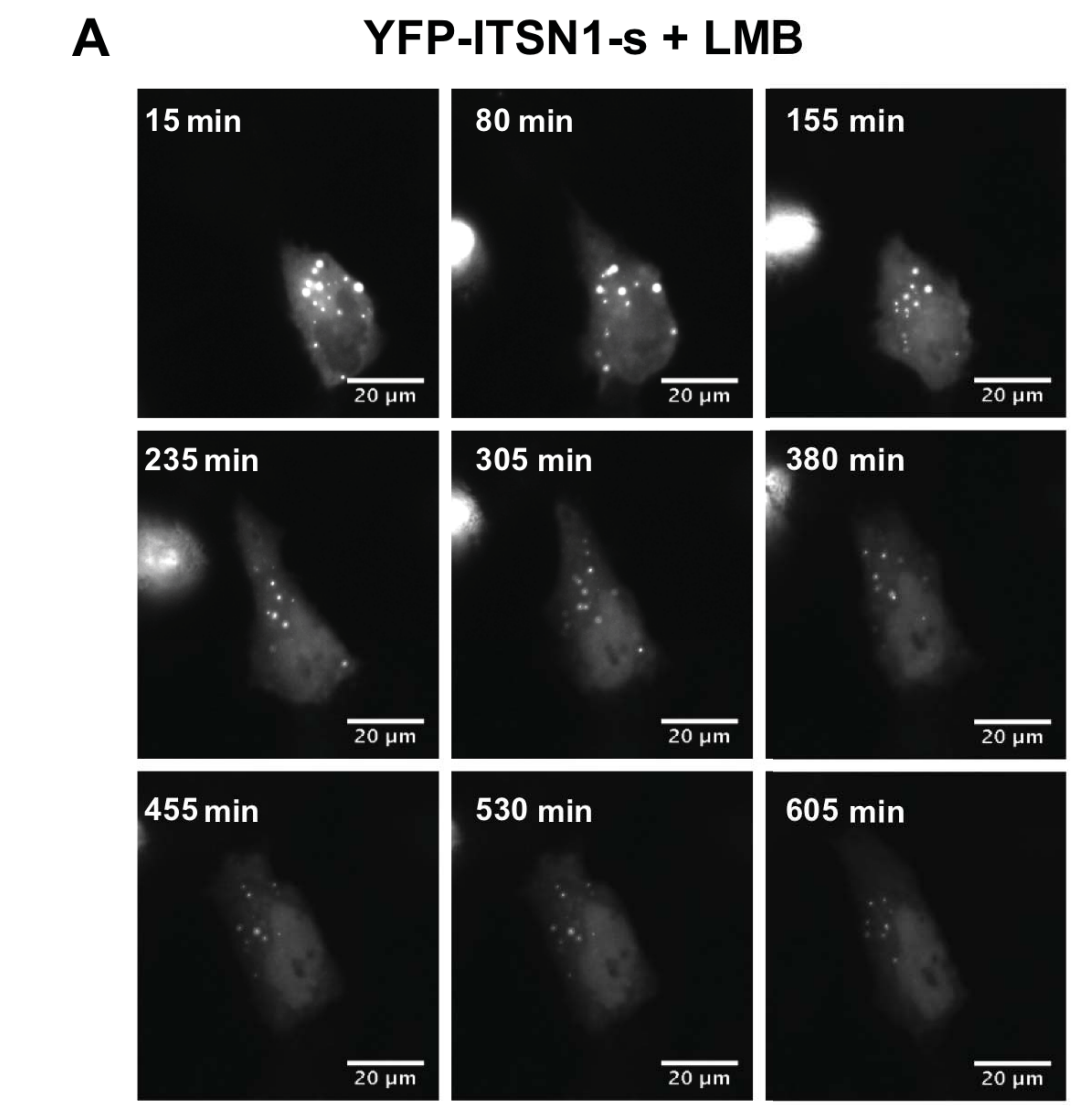
A
YFP-ITSN1-s + LMB
15 min
80 min
155 min
235 min
305 min
380 min
455 min
530 min
605 min
20 µm

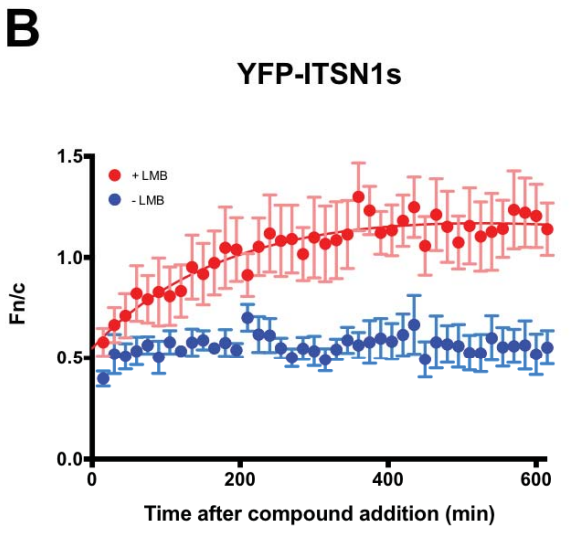
B
YFP-ITSN1s
+ LMB
- LMB
Fn/c
1.5
1.0
0.5
0.0
0
200
400
600
Time after compound addition (min)

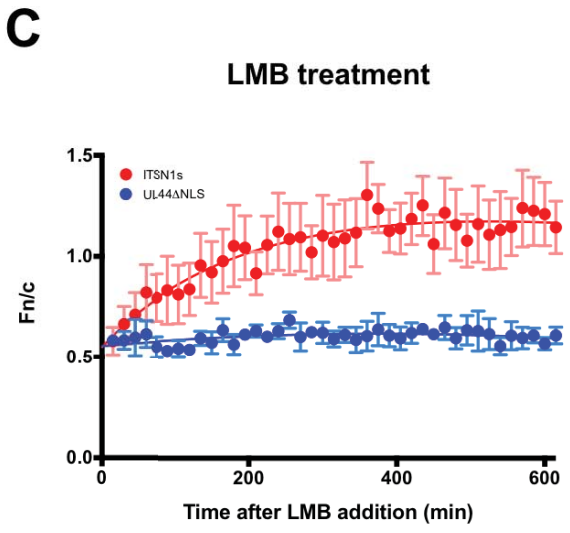
C
LMB treatment
ITSN1s
UL44ΔNLS
Fn/c
1.5
1.0
0.5
0.0
0
200
400
600
Time after LMB addition (min)